

METHODS

A modified TurboID approach identifies tissue-specific centriolar components in *C. elegans*Elisabeth Holzer , Cornelia Rumpf-Kienzl, Sebastian Falk , Alexander Dammermann *

Max Perutz Labs, University of Vienna, Vienna Biocenter (VBC), Vienna, Austria

* alex.dammermann@univie.ac.at

OPEN ACCESS

Citation: Holzer E, Rumpf-Kienzl C, Falk S, Dammermann A (2022) A modified TurboID approach identifies tissue-specific centriolar components in *C. elegans*. PLoS Genet 18(4): e1010150. <https://doi.org/10.1371/journal.pgen.1010150>

Editor: Susan K. Dutcher, Washington University School of Medicine, UNITED STATES

Received: January 14, 2022

Accepted: March 15, 2022

Published: April 20, 2022

Copyright: © 2022 Holzer et al. This is an open access article distributed under the terms of the [Creative Commons Attribution License](https://creativecommons.org/licenses/by/4.0/), which permits unrestricted use, distribution, and reproduction in any medium, provided the original author and source are credited.

Data Availability Statement: Raw mass spectrometry data have been deposited to the ProteomeXchange Consortium via the PRIDE partner repository (<http://www.ebi.ac.uk/pride>) with the dataset identifier PXD031970.

Funding: This work was supported by grants P30760-B28 and P34526-B from the Austrian Science Fund (FWF, <https://www.fwf.ac.at>) to AD. The funders had no role in study design, data collection and analysis, decision to publish, or preparation of the manuscript.

Abstract

Proximity-dependent labeling approaches such as BioID have been a great boon to studies of protein-protein interactions in the context of cytoskeletal structures such as centrosomes which are poorly amenable to traditional biochemical approaches like immunoprecipitation and tandem affinity purification. Yet, these methods have so far not been applied extensively to invertebrate experimental models such as *C. elegans* given the long labeling times required for the original promiscuous biotin ligase variant BirA*. Here, we show that the recently developed variant TurboID successfully probes the interactomes of both stably associated (SPD-5) and dynamically localized (PLK-1) centrosomal components. We further develop an indirect proximity labeling method employing a GFP nanobody-TurboID fusion, which allows the identification of protein interactors in a tissue-specific manner in the context of the whole animal. Critically, this approach utilizes available endogenous GFP fusions, avoiding the need to generate multiple additional strains for each target protein and the potential complications associated with overexpressing the protein from transgenes. Using this method, we identify homologs of two highly conserved centriolar components, Cep97 and BLD10/Cep135, which are present in various somatic tissues of the worm. Surprisingly, neither protein is expressed in early embryos, likely explaining why these proteins have escaped attention until now. Our work expands the experimental repertoire for *C. elegans* and opens the door for further studies of tissue-specific variation in centrosome architecture.

Author summary

‘You can tell a lot about a person by the company they keep.’ This is as true for proteins as it is for people. Unfortunately, the methods traditionally used to probe protein-protein interactions, which rely on isolating stable multimolecular complexes, fail where such complexes do not exist or cannot be isolated from the cell. Proximity-dependent labeling methods such as TurboID, where interacting proteins are marked *in vivo* before isolation and which therefore do not require complexes to be maintained during extract preparation, have consequently become invaluable tools in cell biology. Normally, this requires

Competing interests: The authors have declared that no competing interests exist.

the protein of interest to be tagged with an enzymatic marker such as the biotin ligase BirA*. Here, we developed a variant of this method, whereby the enzyme is targeted to the protein of interest using a genetically-encoded GFP nanobody, making existing fluorescent strains immediately available for interaction biochemistry. We show that this method successfully probes protein-protein interactions in a tissue-specific manner, even where those interactions occur in only a few cells in the context of the entire animal. While this work was conducted in the nematode *C. elegans*, the same method should be applicable to other genetic experimental models, as well as potentially vertebrate cultured cells.

Introduction

Studies in the nematode *C. elegans* have contributed greatly to our understanding of centrosome biology, with comprehensive genome-wide screens leading to the identification of the conserved molecular machinery underlying centriole assembly as well as key players in mitotic pericentriolar material (PCM) recruitment, aided by the strong and reproducible phenotypes observed following RNAi-mediated depletion in the early embryo [1,2]. The striking success of biochemical approaches reconstituting elements of centriole and PCM assembly *in vitro* underline the power of this experimental model [3–6]. The assumption here is that we have a complete parts list of all essential components of centrosomal structures. Recent work identifying further centriolar and pericentriolar material components whose depletion phenotypes are somewhat more subtle [7–9] suggests this is not necessarily the case. Furthermore, while most of the work in *C. elegans* has focused on the early embryo, the available data for the acentriolar centrosome at the ciliary base of sensory neurons [10,11] and the non-centrosomal microtubule organizing center in the intestine [12,13] (Fig 1A) hints at tissue-dependent differences in centrosome composition and assembly mechanisms in somatic tissues of the worm that as yet remain little explored.

Interaction proteomics potentially offers an alternative strategy to identify novel components of centrioles and centrosomes in different tissues of the worm. However, traditional approaches to probing cytoskeletal protein-protein interactions have been hampered by the fact that these interactions mostly take place in the context of the fully assembled structure, with few soluble cytoplasmic pre-complexes available for isolation by immunoprecipitation or other biochemical methods [14]. Proximity-dependent methods circumvent this problem by direct labeling of interacting/proximal proteins, eliminating the need to preserve protein-protein interactions during extract preparation [15]. BioID has revolutionized vertebrate centrosome biology [16–18] but hitherto has not been applied to worms (or flies) due to the low activity of the original promiscuous biotin ligase BirA* requiring long labeling times (~24 hours) incompatible with the rapid development of invertebrate model organisms. The variant TurboID reduces this time to as little as 10 min and indeed this tool was developed specifically for use in *C. elegans* and *Drosophila* [19]. Here, we examine the potential for TurboID to probe the interactomes of both stably associated and dynamically localized centrosomal components in *C. elegans* embryos. We further develop an indirect proximity labeling method and use it to gain initial insights into the tissue-specific variation in centrosome composition in the worm, identifying several proteins expressed exclusively at later developmental stages, including potential homologs of two highly conserved centriolar components, Cep97 and BLD10/Cep135.

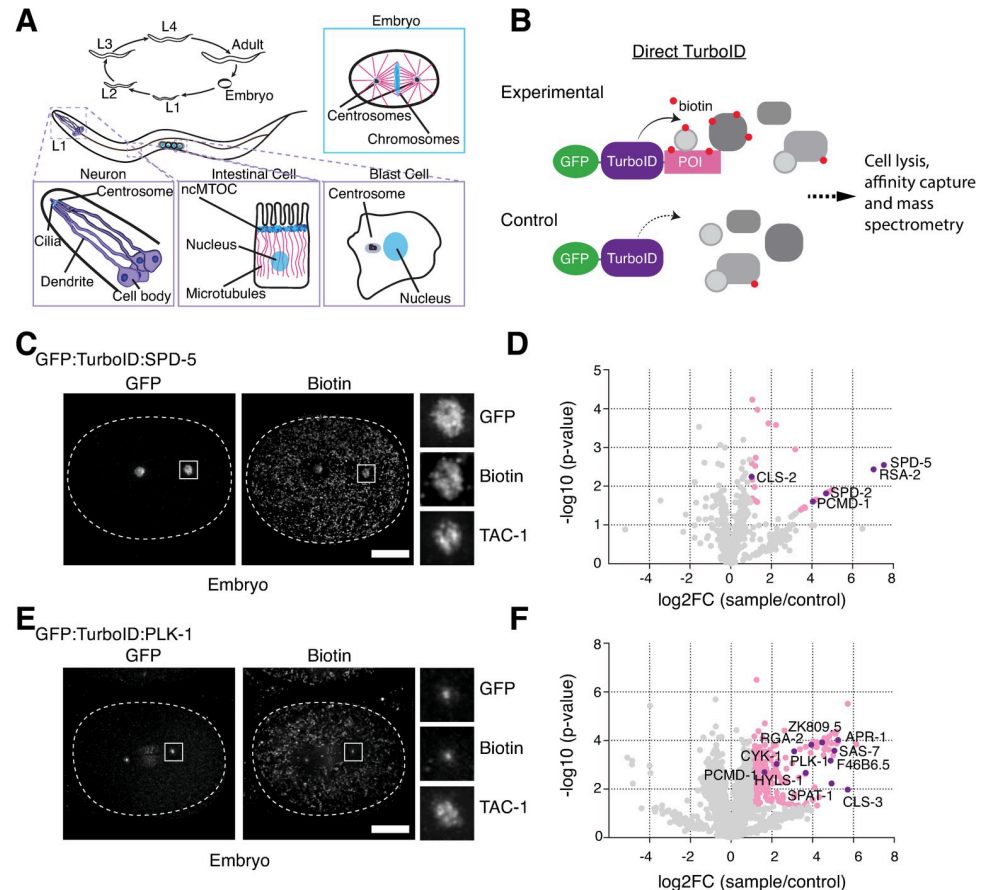


Fig 1. Probing the proximity interactome of centrosomal proteins by TurboID. (A) Centrosomes and centrosome-related structures in *C. elegans*. Centrosome assembly and function has been primarily examined in the early embryo, although some limited work has also been performed on the acentriolar centrosome at the ciliary base of sensory neurons [10, 11] and the non-centrosomal microtubule organizing center in the intestine [12,13]. Blast cells are two pairs of cells in the L1 larva that will give rise to the somatic gonad and germline in the adult worm. At the L1 larval stage these cells are arrested in G1 and G2 phase of the cell cycle, respectively, with what appear to be canonical interphase centrosomes [60,61]. (B) Schematic of direct TurboID [19] which in our implementation also includes a GFP tag to visualize the TurboID fusion. Note that experimental and control TurboID fusions (lacking the protein of interest, POI) are expressed as separate transgenes, though under the same promoter and 3' regulatory sequences. (C) TurboID applied to the PCM scaffolding protein SPD-5. Immunofluorescence micrograph of early embryo expressing GFP:TurboID:SPD-5 stained for GFP, biotin (streptavidin) and TAC-1 as a PCM countermarker. Biotinylation signal is observed at centrosomes without supplemental biotin addition. (D) Result of LC-MS/MS analysis for direct TurboID on SPD-5 from mixed-stage embryos. Volcano plot of $-\log_{10}$ p-values against \log_2 fold change (sample/control). Significantly enriched proteins (\log_2 enrichment >1 , p-value <0.05) are indicated in pink, with selected proteins highlighted. See also S1 Table and S2C Fig. (E) TurboID applied to the dynamically localized PCM regulator PLK-1. Immunofluorescence micrograph of early embryo expressing GFP:TurboID:PLK-1 stained for GFP, biotin (streptavidin) and TAC-1 as a PCM countermarker. Biotinylation signal is observed at centrioles coincident with GFP:PLK-1 signal. (F) Result of LC-MS/MS analysis for direct TurboID on PLK-1 from mixed-stage embryos. See also S1 Table and S2D Fig. Scale bars in C and E are $10\mu\text{m}$.

<https://doi.org/10.1371/journal.pgen.1010150.g001>

Results and discussion

Establishment of TurboID proximity-dependent labeling to probe centrosome architecture in *C. elegans*

When we set out on this project TurboID had not yet been successfully applied to identify the proximity interactors of specific proteins in *C. elegans* (two such studies were recently published by the Feldman and de Bono labs, [13,20]). To explore the potential for TurboID to map

centrosomal protein-protein interactions we chose two target proteins for our proof of principle experiments, the PCM scaffolding protein SPD-5 and the Polo-like kinase PLK-1. As the major structural component of centrosomes in *C. elegans* [6,21], SPD-5 displays no detectable exchange with the cytoplasmic pool once incorporated into the centrosome [22]. Moreover, fluorescence correlation spectroscopy has shown that SPD-5 is largely monomeric in the cytoplasm, with only a small fraction associated with the PP2A regulatory proteins RSA-1 and RSA-2 [14]. Consistent with this, our efforts to identify SPD-5 interactors by tandem affinity purification using the localization and affinity purification (LAP) tag [23] were unsuccessful. In contrast, Plk1 dynamically localizes to multiple mitotic structures, with almost complete exchange at centrosomes within seconds after photobleaching. A key regulator of mitotic events, its behavior is thought to be the result of transient interactions with its numerous substrates throughout the cell [24,25]. SPD-5 and PLK-1 both therefore in different ways represent challenging subjects for interaction biochemistry. We began by generating transgenic strains for each protein expressing a GFP-TurboID fusion under endogenous regulatory sequences by Mos1 transposon mediated insertion at a defined chromosomal locus [26], along with corresponding control strains lacking the SPD-5/PLK-1 coding sequence (Fig 1B). Both fusions localized similarly to the endogenous protein in early embryos, with GFP:TurboID:SPD-5 distributed throughout the PCM while GFP:TurboID:PLK-1 was heavily concentrated at centrioles as well as at other cellular locations, including kinetochores and the spindle midzone (Fig 1C and 1E). Fluorescent streptavidin probes showed biotinylation signal coincident with GFP fluorescence in the same locations, indicating functionality of the biotin ligase. In contrast, there was little biotinylation signal in control strains beyond weak mitochondrial staining also seen in N2 wild-type embryos. Interestingly, biotinylation staining, both specific and non-specific, was not noticeably increased upon addition of supplemental biotin, nor were there any deleterious consequences to growing TurboID strains on biotin-producing OP50 bacteria (Embryonic viability 99.4%, n = 1890, GFP:TurboID:SPD-5; 99.9%, n = 2622 GFP:TurboID:PLK-1). We therefore performed *C. elegans* liquid cultures and embryo isolations under standard conditions, with three independent replicates for both experimental (GFP:TurboID:SPD-5/PLK-1) and control (GFP:TurboID) conditions.

In order to enrich for centrosomal interactors, crude embryo extracts were separated into soluble (cytoplasmic) and insoluble (cytoskeletal) fractions, the latter containing the centrosomes as confirmed by characteristic foci of GFP signal when examined under the fluorescence microscope. Centrosomal pellets were then resolubilized under denaturing conditions and used for streptavidin pulldowns followed by LC-MS/MS analysis. As also noted by Artan et al. [20] endogenously biotinylated carboxylases represent a significant proportion of the isolated peptides. However, they, along with other common contaminants including vitellogenins and mitochondrial proteins, are largely filtered out by considering only those proteins significantly enriched in experimental samples over controls (Log₂ enrichment >1, p-value <0.05). What remains for SPD-5 is a remarkably short list, 30 proteins (Fig 1D and S1 Table). By far the most enriched proteins are SPD-5 itself along with its interacting partner RSA-2, though somewhat surprisingly not the PP2A complex of RSA-1, PAA-1 and LET-92 with which SPD-5 has been reported to interact in the cytoplasm via RSA-2 [27], none of which were detected in the prep. Also highly enriched are SPD-2, which contributes to SPD-5 self-assembly *in vitro* [6] and centrosome maturation *in vivo* [28,29], and the recently described PCM tethering factor PCMD-1 [7]. The SPD-2 recruitment factor SAS-7 [8], also highly enriched, just failed the significance threshold, while the remaining proteins are either uncharacterized or likely contaminants (Fig 1D and S1 Table). The list of SPD-5 proximity interactors therefore consists primarily of proteins related to PCM scaffold assembly. Notably absent are other centriolar and PCM components, including highly abundant ones such as γ -tubulin (TBG-1 in *C.*

elegans) [30]. TurboID, then, is highly specific with a labeling radius narrower than the 10–15 nm estimated for BirA* [31]. The list for PLK-1 is considerably longer, 235 proteins, including numerous proteins involved in cytoskeletal organization and morphogenesis, such as CLS-3/CLASP [32], CYK-1 [33], RGA-2 [34], APR-1/APC [35] and several uncharacterized proteins reported to interact with PLK-1 in high-throughput screens (F46B6.5, ZK809.5, [36,37]) (Fig 1F and S1 Table). Also present is the PLK-1 activator SPAT-1/Bora [38]. In contrast, just three centrosomal proteins make the list, HYLS-1, PCMD-1, and SAS-7, like PLK-1 all centriolar proteins. HYLS-1 has no known link to PLK-1 or PCM recruitment [39]. However, both SAS-7 [8] and PCMD-1 [7] are required for centrosomal PLK-1 recruitment, directly or indirectly via SPD-2. TurboID thus also identifies meaningful proximity interactors of dynamically localized proteins, although the higher number of hits overall makes it difficult to isolate novel proteins without additional information to prioritize specific candidates. We conclude that TurboID successfully identifies cytoskeletal protein interactors in *C. elegans*, albeit with notably better results for stably associated centrosomal components.

GFP nanobody-directed TurboID as an improved method for proximity-dependent labeling

Direct TurboID tagging as described above carries with it certain disadvantages. First, to eliminate common contaminants, two TurboID strains need to be generated for each target protein, requiring a significant investment of time and effort. Moreover, those two TurboID constructs will usually be expressed as transgenes. While endogenous tagging can be carried out [20], it is then difficult to generate a corresponding control matching the expression level of the TurboID-protein fusion, important for normalization of the MS data. Expression level is a particular concern when aiming to isolate proximity interactors of a protein in a specific cell type or tissue, since the relevant promoters will not necessarily match the expression level of the endogenous protein. This is assuming that the fusion protein will be able to integrate into its normal cellular context, which for centriolar proteins, often stably incorporated in previous cell cycles, will not necessarily be the case [40]. Our aim was to develop an optimized tool for proximity-dependent labeling that minimizes strain generation and is able to utilize endogenous proteins, even in a cell/tissue-specific context. Rather than directly tagging the protein of interest, our approach was to express a TurboID fusion as a transgene under a ubiquitous or tissue-specific promoter and target it to the (endogenously GFP-tagged) protein of interest using a GFP nanobody [41] (Figs 2A and S1). Such endogenous GFP fusions will frequently already be available for proteins under study. The same GFP nanobody-TurboID promoter construct can then be used for multiple different target proteins by crossing it into the relevant GFP strain background and, when expressed alone, serves as an expression-matched control for mass spectrometry sample normalization. It should be noted that a similar strategy was recently developed for use in zebrafish [42], albeit employing a conditionally stabilised GFP-binding nanobody, with implications for sample normalization as discussed below.

To test our approach, we generated a strain expressing the GFP nanobody-TurboID fusion under the germline promoter *pie-1* and crossed it with strains expressing endogenously GFP-tagged SPD-5 and PLK-1. In both cases, immunofluorescence microscopy showed biotinylation signal colocalizing with the GFP-tagged protein, in the case of SPD-5 in the PCM and in the case of PLK-1 at centrioles, kinetochores and the spindle midzone (Fig 2C and 2E). Indeed, this signal was significantly (3–10x) stronger than that for direct TurboID, making the (unchanged) cytoplasmic background appear less prominent. The GFP nanobody therefore successfully penetrates the centrosome and directs the biotin ligase to the appropriate intracellular location. The GFP nanobody-TurboID fusion is fairly large (a combined 50kDa for

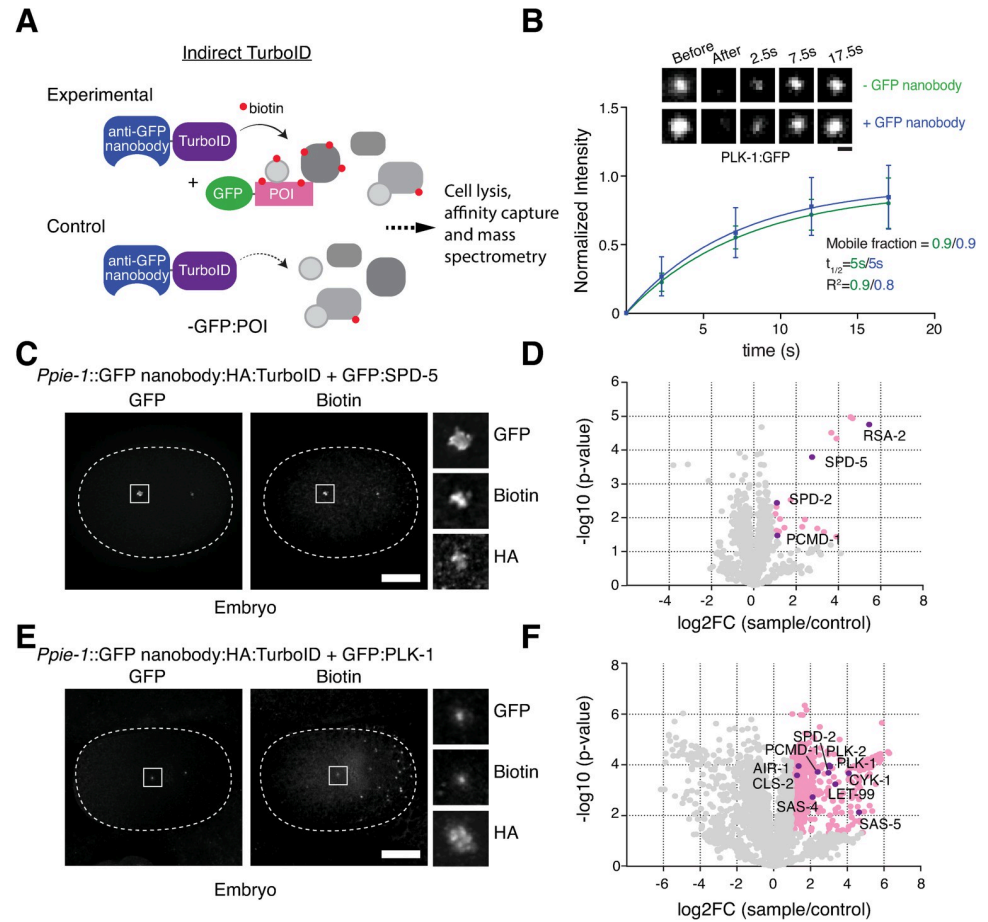


Fig 2. GFP nanobody-directed TurboID as an improved method for proximity-dependent labeling. (A) Schematic of indirect TurboID method, whereby the biotin ligase is targeted to an endogenous GFP fusion via a GFP nanobody [41]. Note that experimental and control strains utilize the same TurboID fusion, which may be expressed under a tissue or developmental stage-specific or inducible promoter, while the target protein is potentially expressed in a wide array of tissues and cell types. (B) GFP nanobody addition does not perturb PLK-1 mobility. Selected images and quantitation for fluorescence recovery after photobleaching (FRAP) analysis performed on PLK-1:GFP at centrosomes in prometaphase-stage embryos in the presence ($n = 16$ animals) or absence ($n = 13$) of the GFP nanobody:TurboID fusion. (C) Indirect TurboID applied to SPD-5. Immunofluorescence micrograph of early embryo from strain co-expressing a GFP nanobody:HA:TurboID fusion under the germline promoter *pie-1* and endogenously GFP-tagged SPD-5 stained for GFP, biotin (streptavidin) and HA. Biotinylation signal is observed at centrosomes coincident with GFP:SPD-5 and the TurboID fusion. (D) Result of LC-MS/MS analysis for indirect TurboID on SPD-5 from mixed-stage embryos. Volcano plot of $-\log_{10}$ p-values against \log_2 fold change (sample/control). Significantly enriched proteins (\log_2 enrichment > 1 , p-value < 0.05) are indicated in pink, with selected proteins highlighted. Compare Fig 1D. See also S1 Table and S2E Fig. (E) Indirect TurboID applied to PLK-1. Immunofluorescence micrograph of early embryo from strain co-expressing a GFP nanobody:HA:TurboID fusion under the germline promoter *pie-1* and endogenously GFP-tagged PLK-1 stained for GFP, biotin (streptavidin) and HA. Biotinylation signal is observed at centrosomes coincident with PLK-1:GFP and the TurboID fusion. (F) Result of LC-MS/MS analysis for indirect TurboID on PLK-1 from mixed-stage embryos. Compare Fig 1F. See also S1 Table and S2E Fig. Scale bars are $1\mu\text{m}$ (B), $10\mu\text{m}$ (C, E).

<https://doi.org/10.1371/journal.pgen.1010150.g002>

nanobody and ligase), which when added to the 27kDa of GFP could perturb the dynamics or functionality of the target protein. However, both double strains were found to be fully viable (Embryonic viability 98.6%, $n = 1209$, GFP:SPD-5 and GFP nanobody-TurboID; 99.6%, $n = 1614$, GFP:SPD-5 alone; 99.6%, $n = 2355$, GFP:PLK-1 and GFP nanobody-TurboID; 98.4%, $n = 1512$, GFP:PLK-1 alone). In addition, we assessed the dynamics of cytoplasmic exchange of GFP:PLK-1 at centrosomes by fluorescence recovery after photobleaching in

prometaphase-stage embryos in the presence and absence of the nanobody. As previously reported for vertebrate somatic cells [24,25] cytoplasmic exchange of PLK-1 is extremely rapid, with a half-time of recovery $t_{1/2}$ of 5s, with essentially no stably associated centriolar or PCM population (mobile fraction $A = 0.9$). These dynamics remained unchanged in the presence of the nanobody (Fig 2B). Nanobody addition therefore does not appreciably hinder localization, dynamics or functionality of the target protein.

While we were able to detect biotinylation signal at centrosomes with both GFP fusions, we sought to compare labeling efficiency of direct and indirect TurboID approaches. We therefore prepared cytoskeletal fractions from embryo extracts and performed mass spectrometry on streptavidin pull-downs as for direct TurboID, with three independent replicates for both experimental (GFP nanobody-TurboID and GFP:SPD-5/PLK-1) and control (GFP nanobody-TurboID only) conditions. One might expect that the insertion of two additional elements between biotin ligase and target protein (GFP nanobody and GFP) would widen the resultant labeling radius around the target protein. However, results were broadly similar compared to direct TurboID. In the case of SPD-5, the list of proteins significantly enriched in experimental samples over controls actually shrunk, to 22 proteins (Fig 2D and S1 Table). With one exception (SAS-7, not detected in these mass spec samples) the same centrosomal proteins were again found to be enriched, SPD-5 itself, RSA-2, SPD-2 and PCMD-1, with the remainder of the list either uncharacterized proteins or likely contaminants. Only one of these proteins was found on both lists, B0001.2, a nematode-specific protein reported to be required for embryonic development [43] but otherwise currently uncharacterized. For PLK-1, the list was even longer than for direct TurboID, 501 proteins, again comprising many proteins involved in cytoskeletal organization and morphogenesis (Fig 2F and S1 Table). Notably, only 22 proteins were common to both lists, including PCMD-1 (HYLS-1 and SAS-7 were not detected in these samples). There were, however, several additional centrosomal components, including SAS-4 (CPAP/CenpJ in vertebrates), a Plk1 target in mitotic entry [44], and SPD-2 and AIR-1, involved in centriolar recruitment and activation of PLK-1 [45–47]. GFP nanobody-direct TurboID thus performs similarly to direct TurboID in identifying functionally relevant proximity interactors.

Efficient tissue-specific labeling using GFP nanobody-directed TurboID

Our goal in developing GFP nanobody-direct TurboID was not only to simplify and streamline proximity labeling by utilizing available GFP fusions, but to be able to better probe protein-protein interactions in a tissue- or cell-specific context. To evaluate the suitability of our tool for these purposes, we turned to post-mitotic sensory neurons and the acentriolar centrosome at the ciliary base, whose assembly and function we recently investigated [10]. For this we generated a strain expressing the GFP nanobody-TurboID fusion under the ciliated neuron-specific promoter *osm-6* and crossed it into the strain expressing endogenously GFP-tagged SPD-5 (PLK-1 not being expressed in post-mitotic sensory neurons [10]). As in the early embryo, immunofluorescence microscopy showed biotinylation signal colocalizing with the GFP-tagged protein at the ciliary base (Fig 3A). The extended dendrite of these neurons (60 μ m in the L1 larval stage and nearly double that in the adult worm [48]) therefore does not present an obstacle for nanobody targeting.

Ciliated neurons account for only 60 of the 959 somatic cells of the adult hermaphrodite [49], not counting the two gonad arms which harbor numerous germline nuclei within a common syncytium, maturing oocytes, sperm and fertilized embryos. To maximize ciliated neuron representation within the starting material for TurboID, we therefore chose the L1 larval stage (558 cells total [50]), a stage where ciliogenesis is largely complete [51] and which can

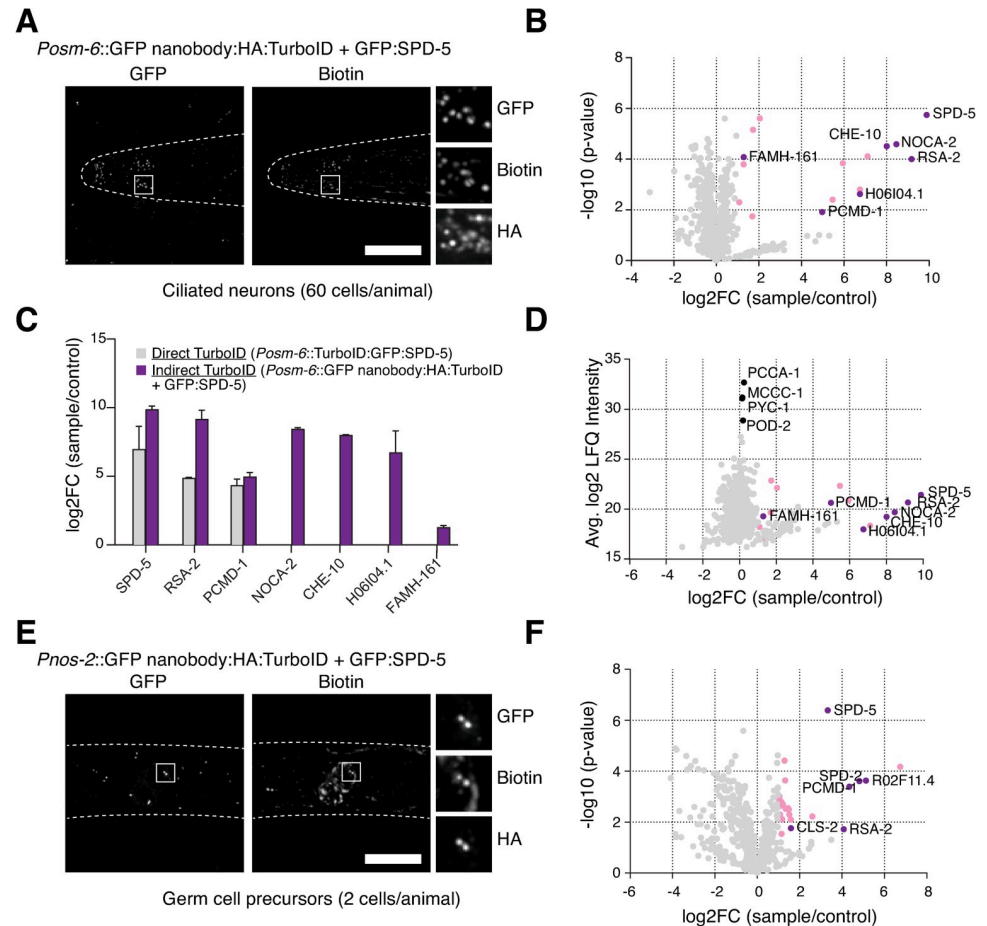


Fig 3. Tissue-specific labeling using GFP nanobody-directed TurboID. (A) TurboID applied to SPD-5 in ciliated neurons. Immunofluorescence micrograph of head of L1 larva from strain co-expressing a GFP nanobody:HA:TurboID fusion under the ciliated neuron-specific promoter *osm-6* and endogenously GFP-tagged SPD-5 stained for GFP, biotin (streptavidin) and HA. Biotinylation signal is observed at the ciliary base coincident with GFP:SPD-5 and the TurboID fusion. (B) Result of LC-MS/MS analysis for indirect TurboID on SPD-5 in ciliated neurons. Volcano plot of $-\log_{10}$ p-values against \log_2 fold change (sample/control). Significantly enriched proteins (\log_2 enrichment >1 , p -value <0.05) are indicated in pink, with selected proteins highlighted. See also S1 Table. (C) Comparison of LC-MS/MS results for direct and indirect TurboID on SPD-5 in ciliated neurons. Indirect TurboID identifies several additional SPD-5 proximity interactors. Full results for direct TurboID presented in S2A and S2B Fig and S1 Table. (D) Volcano plot of average \log_2 LFQ intensity (sample) against \log_2 fold change (sample/control) for indirect TurboID on SPD-5 in ciliated neurons. Significantly enriched proteins (\log_2 enrichment >1 , p -value <0.05) are indicated in pink, with selected proximity interactors highlighted. Note that these interactors are present at much lower levels in the sample compared to endogenously biotinylated proteins, most notably the carboxylases PCCA-1, PYC-1, POD-2 and MCCC-1 [20], highlighting the importance of proper sample normalization. (E) TurboID applied to SPD-5 in germ cell precursors. Immunofluorescence micrograph of the area of the blast cells in an L1 larva co-expressing a GFP nanobody:HA:TurboID fusion under the germline-specific promoter *nos-2* and endogenously GFP-tagged SPD-5 stained for GFP, biotin (streptavidin) and HA. Biotinylation signal is observed at centrosomes in two cells (the primordial germ cells Z2, Z3) coincident with GFP:SPD-5 and the TurboID fusion. (F) Result of LC-MS/MS analysis for indirect TurboID on SPD-5 in germ cell precursors. See also S1 Table and S2H Fig. Scale bars in A and E are 10 μ m.

<https://doi.org/10.1371/journal.pgen.1010150.g003>

furthermore be obtained in a highly synchronized manner and in large quantities by hatching embryos in liquid culture in the absence of food [52]. Conditions for centrosome isolation from later developmental stages of the worm have not been established. We therefore performed TurboID on whole cell extracts as carried out by Artan et al. [20]. Starved worms were fed with OP50.1 supplemented with 1mM biotin for 2 hours prior to extract preparation to

stimulate centrosome assembly [10] and enhance TurboID-dependent biotinylation [20]. Mass spectrometry revealed a clearly defined set of 16 proximity interactors above the significance threshold, with few obvious contaminants (Fig 3B and S1 Table). These included RSA-2 and PCMD-1, also found as SPD-5 interactors in early embryos, but not SPD-2, a protein lost from centrosomes early in neuronal differentiation [51]. The remainder of the list is comprised for the most part of uncharacterized proteins known from high-throughput studies to be expressed in sensory neurons. The one exception is CHE-10, the *C. elegans* homolog of rootletin, which forms the ciliary rootlet in the region of the degenerated basal body [53] in close proximity to the acentriolar centrosome. FAMH-161, the apparent homolog of vertebrate FAM-161A [54] and B, has been localized to the ciliary base [55] but otherwise remains currently functionally uncharacterized. NOCA-2, related to vertebrate ninein-like protein/Nlp [56], likewise must be considered a strong candidate for ciliary base localization and potential basal body/ciliary centrosome function. Both FAM-161A and Nlp have been shown to play important roles in microtubule nucleation, stability and anchoring in the context of the interphase centriole/centrosome/basal body in vertebrates [56–59], functions that may be conserved in *C. elegans*. Another candidate protein identified by mass spectrometry is H06I04.1, a putative ortholog of Cep135/BLD10 (see below). In an effort to further compare direct and indirect GFP nanobody-directed TurboID, direct TurboID was performed in parallel using the same *osm-6* promoter to drive expression of GFP:TurboID:SPD-5 and the corresponding GFP:TurboID control. Here, direct TurboID performed markedly worse, identifying solely RSA-2 and PCMD-1, as well as the uncharacterized proteins F53G12.4, F48E3.9 and ZK809.5 (all also identified by indirect TurboID), amongst a list of 55 proximity interactors, with the remainder clear contaminants (Figs 3C, S2A, S2B and S1 Table). Indirect TurboID therefore offers clear advantages over conventional direct labeling in this tissue-specific context.

Successful tissue-specific labeling in a limited number of cells

Interaction proteomics is particularly challenging where those interactions occur in a complex source material such as within a limited number of cells in a tissue or animal. We next sought to investigate whether our TurboID was able to detect such interactions using the gonad precursor cells in L1 larvae as a test case. These are two sets of two cells, the somatic gonad precursor cells Z1 and Z4 and the primordial germ cells Z2 and Z3, which through a series of divisions at later developmental stages will give rise to the somatic gonad and germline in the adult, respectively. At the L1 larval stage these blast cells are arrested in G1 and G2 phase of the cell cycle, with what appear to be canonical interphase centrosomes [60, 61]. With centrioles and centrosomes degenerating following terminal differentiation in most somatic tissues [51,62], these cells therefore represent potentially the best model for interphase centrosome assembly in the worm. As a first step towards investigating centrosome composition in those cells, we generated GFP nanobody-TurboID fusions under the control of promoters reported to be active in those cells (*Pehn-3a* Z1/Z4 [63], *Pnos-2* Z2/Z3 [64]) and crossed them into the strain expressing GFP-tagged SPD-5. Immunofluorescence microscopy showed robust centrosomal biotinylation signal for the *Pnos-2* promoter in Z2/Z3 cells (Fig 3E). However, for *Pehn-3a* in Z1/Z4 cells there was considerable cytoplasmic background signal, suggesting a weaker promoter would need to be used. We therefore proceeded only with *Pnos-2* in the primordial germ cells, performing TurboID on whole cell extracts prepared from L1 larvae as described above. Mass spectrometry revealed a set of 24 proximity interactors above the significance threshold. Remarkably, aside from two likely contaminants (titin, *ttn-1*, and *mca-3*, a muscle plasma membrane Ca²⁺ ATPase) the top hits were exclusively centrosomal proteins: SPD-2, PCMD-1, RSA-2 and CLS-2/CLASP [32], as well as R02F11.4, a potential homolog of Cep97

(Fig 3F and S1 Table). We conclude that GFP nanobody-directed TurboID successfully identifies protein proximity interactors, even when interactions occur only in a very limited subset of cells (in this case 2 out of 558 cells). Given the robustness of this dataset compared even with TurboID performed in embryos we propose that sample enrichment (e.g. by fractionation) is not required and may indeed result in less reliable results due to increased variability between replicates.

Cep97 and Cep135/BLD10 as tissue-specific centrosomal components

Cep97 and Cep135/BLD10 are well-known centriolar components with critical roles in centriole assembly/stability and centrosome/cilium biogenesis [65–69]. Cep135 in particular is highly conserved and along with SAS-4 and SAS-6 has been proposed to be one of three proteins defining centriole/basal body architecture across eukaryotes [70]. It is then surprising that both Cep97 and Cep135 have been reported to be absent from the *C. elegans* genome [70,71]. However, it must be noted that nematode genomes are highly divergent such that even conserved components such as PLK4/ZYG-1 were originally reported to be missing based on lack of amino acid sequence homology [70,72] and not recognized as such until much later based on conserved 3D structure and molecular function. Their identification has thus been almost invariably based on genome-wide screens performed for centriole/centrosome assembly in the early embryo and somewhat less comprehensive genetic screens for cilium biogenesis in sensory neurons [1–49].

The identification of R02F11.4 as the ortholog of Cep97 (hereafter named CCEP-97 for *C. elegans* Centrosomal Protein of 97kDa) is quite clear to the extent of being annotated as such on Wormbase (Version WS282, November 2021), although it does require the use of intermediary, less divergent, species for successive reciprocal BLAST identification or Position-Specific Iterated BLAST (PSI-BLAST) analysis (S3A and S3B Fig). 3-dimensional structure prediction via AlphaFold [73] also suggests a similar protein architecture of the *C. elegans*, *Drosophila* and human proteins, including a leucine rich repeat region and extended coiled coils (Fig 4A). Generation of an endogenous promoter GFP transgene revealed CCEP-97 localization to centrioles in late-stage embryos, gonad precursors and the ciliary base (Fig 4B), but not in early embryos or at the non-centrosomal microtubule organizing center of embryonic intestinal cells (S3C Fig). This is consistent with the lack of a reported early embryo RNAi phenotype in high-throughput screens, a result we have confirmed in our own hands (Embryonic viability 99.6%, $n = 1219$, *ccep-97(RNAi)*; 1.1%, $n = 1272$, *spd-5(RNAi)*; 99.8%, $n = 1238$, Control). However, a partial gene deletion (*tm4945*) results in fully penetrant L1 larval arrest, suggesting a critical role in later development. Further experiments will be necessary to define CCEP-97 function in the worm. However, it is striking to note that CCEP-97 is first detectable at centrioles as the cell cycle slows in late-stage embryos and strongly accumulates at centrioles in gonad precursor cells, cells which as previously noted are arrested for extended periods of time in interphase. These findings are consistent with recent reports of cell cycle-entrained oscillations of Cep97 levels regulating centriole growth in *Drosophila* [74].

H06I04.1 (hereafter CCEP-135) initially caught our attention as a putative interactor of the centriolar proteins SAS-6, FAMH-161/FAM161A/B and NOCA-2/NINL, as well as the microtubule-associated protein ZYG-8/Doublecortin, in high-throughput screens [75,76]. Direct BLAST searches initially failed to identify any homologs outside of nematodes. However, repeated rounds of Position-Specific Iterated BLAST (PSI-BLAST) identified homologs first in insects and then vertebrates, all related to Cep135/BLD10 (S4A and S4B Fig). Amino acid sequence conservation is clearly very low. However, *C. elegans*, *Drosophila* and human proteins all contain multiple predicted coiled coils, which for human Cep135 have been shown to

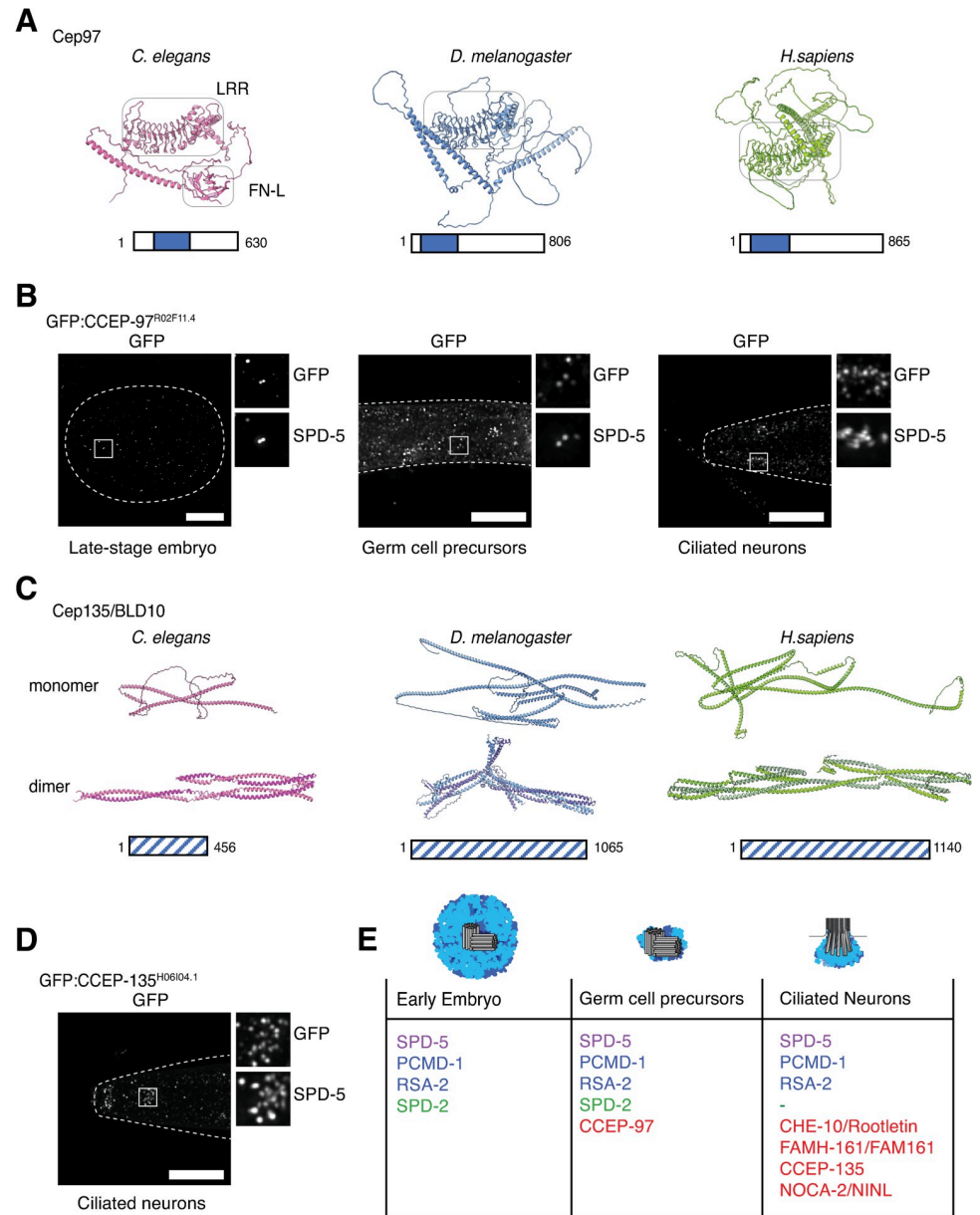


Fig 4. CCEP-97 and CCEP-135 as novel tissue-specific centrosomal components in *C. elegans*. (A) AlphaFold [73] predicts a similar 3D architecture for *C. elegans* R02F11.4/CCEP-97 and its putative *Drosophila* and human orthologs Cep97, including a prominent leucine rich repeat that is highly conserved across Cep97 orthologs followed by long coiled coils (see S3A and S3B Fig). Additionally, a Fibronectin type III (FN-3) domain is predicted for the *C. elegans* protein, which is conserved in other nematode homologs but not in insects or vertebrates. (B) An endogenous promoter GFP transgene shows CCEP-97 to be expressed in late-stage embryos, germ cell precursors and ciliated neurons, localizing to centrioles (marked by immunofluorescence co-staining with SPD-5) and the ciliary base (likewise), respectively. (C) AlphaFold structure prediction shows *C. elegans* H06I04.1/CCEP-135 and its putative *Drosophila* and human orthologs Cep135/BLD10 to display a similar 3D architecture, composed primarily of coiled coils. These align in a rope-like manner when predicting the proteins to form dimers as has been shown for human and *Chlamydomonas* Cep135/BLD10 [77]. For hsCep135 and dmCep135 only the N-terminal regions (1–600, hsCep135; 1–547, dmCep135) were used for homodimer prediction to reduce computational costs. We note that in the homodimeric dmCep135 model some regions are overlapping suggesting that the native structure deviates from the prediction. For CCEP-135 the first 131 residues, predicted with lower confidence, are not displayed. See also S4A and S4B Figs. (D) An endogenous promoter GFP transgene shows CCEP-135 to be expressed in ciliated sensory neurons of the head (amphids and cephalic/labial neurons), localizing to the ciliary base (marked by immunofluorescence co-staining with SPD-5). (E) Comparison of selected SPD-5 proximity interactors identified in embryos, germ cell precursors and ciliated neurons (for full list see S1 Table). Common to all three tissue contexts are

PCMD-1 and RSA-2, while SPD-2 is absent from post-mitotic sensory neurons. The previously uncharacterized proteins CCEP-97 and CCEP-135 are amongst the tissue-specific SPD-5 interactors, identified in germ cell precursors and ciliated neurons, respectively. Scale bars in B and D are 10 μ m.

<https://doi.org/10.1371/journal.pgen.1010150.g004>

be important for dimerization and microtubule binding [77] (Fig 4C). An endogenous promoter GFP transgene revealed CCEP-135 expression exclusively in post-mitotic neurons, where it localizes to the ciliary base (Fig 4D), as well as the nerve ring. No clear signal was observed elsewhere in the worm or in early embryos (S4C Fig), consistent with the lack of a reported RNAi phenotype in high-throughput screens and our own hands (Embryonic viability 99.9%, n = 1715, *ccep-135(RNAi)*). CCEP-135 would thus appear to function specifically in the context of centriole-derived basal bodies. While Cep135 is generally thought of as a cartwheel component important for centriole assembly [67], a more limited function in the context of cilia would be consistent with work in *Drosophila*, where it is basal bodies and consequently cilia that are primarily affected in Cep135 mutants [67,68,78].

Conclusions and outlook

Proximity labeling by BioID has provided valuable insights into the molecular composition of centrosomes and related structures in vertebrate cells [16–18]. The recent development of TurboID [19] promises to do the same for invertebrate experimental models like *C. elegans* and *Drosophila*. The indirect GFP nanobody-directed TurboID approach developed here represents a refinement of this method, which in genetic models greatly simplifies strain generation by allowing the repurposing of existing GFP-tagged strains for TurboID. More importantly, when not combined with the GFP fusion of interest the GFP nanobody-TurboID strain represents the ideal expression-matched control to remove non-specific background and identify *bona fide* proximity interactors in the often extensive mass spectrometry lists. This superior ability to filter mass spectrometry data is demonstrated by strikingly successful tissue-specific labeling, even when the bait is expressed in only a highly limited number of cells, such as the germ cell precursors. Abundant endogenously biotinylated proteins, including the carboxylases PCCA-1, PYC-1, POD-2 and MCCC-1 noted by Artan et al. [20], do represent a significant proportion of the isolated peptides (see Fig 3D), but can be easily filtered out. Enriching for a specific cell type or intracellular structure of interest as we did by fractionation of embryo extracts is therefore clearly not necessary and may actually result in less reliable results due to increased variability between replicates. As previously noted, a similar approach employing a conditionally stabilised GFP-binding nanobody was recently developed for use in zebrafish [42]. In this approach, the GFP nanobody-TurboID fusion is destabilized when not bound to the protein of interest, reducing non-specific labeling. However, this also compromises the ability to use the GFP nanobody-TurboID fusion alone as an expression-matched control for mass spectrometry data normalization. Regardless of their individual advantages and disadvantages, both strategies clearly hold great promise in tackling previously inaccessible problems in interaction proteomics across genetic models from *C. elegans* to vertebrates. The use of inducible promoters in combination with indirect TurboID should further expand the scope of possible proximity labeling experiments, something we have not explored here.

Contrary to common perception, proximity labeling by TurboID appears to be highly restricted, identifying only those proteins in closest proximity to the bait protein. In the case of SPD-5, these are proteins like PCMD-1, SPD-2 and RSA-2, all of which are known to interact with SPD-5 and regulate PCM assembly (see below). Other PCM proteins including highly abundant ones like γ -tubulin are not detected, suggesting a labeling radius even more narrow than the 10–15 nm previously estimated for BioID [31]. This method is therefore ideally suited

for the identification of potential protein-protein interactors, but perhaps less so for compartment labeling, even when using a bait protein found throughout a structure of interest such as the PCM. In comparison with our results for SPD-5, a stably bound component of the PCM scaffold [22], our results for the dynamically localized kinase PLK-1 were markedly less clear, with extensive background requiring strategies to prioritize hits and identify true proximity interactors. Performing additional replicates or combining multiple baits may help make sense of such more complex data.

In this proof of principle study, we applied our tool to carry out an initial characterization of tissue-dependent variation in PCM composition in the worm, focusing on proximity interactors of the scaffolding component SPD-5 in embryos, germ cell precursors and at the ciliary base (Fig 4E). Our data identify RSA-2 and PCMD-1 as SPD-5 proximity interactors common to all three developmental contexts. PCMD-1 is perhaps not a surprise, having been found to contribute to SPD-5 recruitment/tethering to centrioles in the early embryo and the ciliary base in sensory neurons [7,10,79], RSA-2 somewhat more so. While RSA-2 was originally identified as a centrosomal PP2A recruitment factor [27], its proximity interaction with SPD-5 at all types of centrosomes in the apparent absence of the phosphatase suggests a more direct role in the regulation of PCM assembly which bears closer investigation. There is also considerable tissue-dependent variation in PCM composition. Thus, SPD-2 is only detected in mass spectrometry samples for SPD-5 in embryos and germ cell precursors, but not sensory neurons, consistent with the previously reported loss of SPD-2 from the acentriolar centrosome at the ciliary base [10,51]. Other proteins are only detected at later developmental stages, such as CCEP-97. Its appearance at centrioles in late-stage embryos may reflect a slowing of the cell cycle allowing its accumulation during the more extended interphase [74], and be connected to the emergence of centriolar doublet microtubules at approximately the same time [51,80]. Finally, ciliated sensory neurons present a unique set of SPD-5 proximity interactors, including CHE-10/rootletin. A surprising finding here is the identification of a homolog of Cep135/BLD10, previously thought to be missing in nematodes, present exclusively at the ciliary base. Further work will be needed to clarify the functional contribution of this protein to basal body architecture and cilium assembly in *C. elegans*, but this tissue-specific expression pattern is consistent with a role for this protein specifically in the context of cilia [67,68,78].

In summary, then, our data suggest that centrioles and centrosomes may be much more variable across different tissues and developmental stages than currently appreciated. The systematic application of newly developed tools such as tissue-specific TurboID and inducible degron-mediated degradation to investigate their molecular composition and the underlying molecular mechanisms at work should help shed light on what has hitherto been a somewhat neglected aspect of centrosome biology.

Materials and methods

Experimental model and subject details

***C. elegans* strains and culture conditions.** *C. elegans* strains expressing endogenously tagged GFP:SPD-5 [45] and PLK-1:GFP [81] and endogenous promoter-driven TBG-1:mCherry [82] have been described previously. Strains expressing endogenous promoter-driven GFP:TurboID:SPD-5 and GFP:TurboID:PLK-1 and *Posm-6*-driven TurboID:GFP:SPD-5, as well as corresponding control strains lacking the SPD-5/PLK-1 coding sequence, were generated by cloning the corresponding genomic locus including 5' and 3' regulatory sequences, GFP and TurboID into the targeting vector pCFJ151, followed by *Mos1*-mediated transposition [26]. SPD-5 and GFP coding sequence were derived from plasmid pAD395 [83], TurboID from plasmid pAS31 [19]. All other fragments were amplified from *C. elegans*

genomic DNA (length of *spd-5* promoter 1150bp, 3'UTR 577bp; *plk-1* promoter 2000bp, 3'UTR 2324bp; *osm-6* promoter 425bp). Strains expressing the GFP nanobody-TurboID fusion under various tissue-specific 5' and 3' regulatory sequences were generated by Mos1 transposon insertion as above. HA tagged-TurboID was derived from plasmid pAS31 [19], the GFP nanobody from plasmid pAD834 [10]. Promoters and 3'UTRs were amplified from plasmids pCFJ152 (*pie-1* promoter, 1105bp, [26]) and pAD834 (*tbb-2* 3'UTR, 330bp [10]), as well as *C. elegans* genomic DNA (*osm-6* promoter 425bp; *nos-2* promoter, 956bp, 3'UTR, 1000bp; *ehn-3a* promoter, 2004bp, 3'UTR 806bp). *pie-1* promoter-driven GFP nanobody-TurboID is also combined with mCherry:histone H2B as a visible marker co-expressed via an operon linker, amplified from plasmid pLC754 (gift from Luisa Cochella, [84]). Strains expressing endogenous promoter-driven GFP:CCEP-97 and GFP:CCEP-135 were generated by Mos1 transposon insertion as above. In each case promoter (*ccep-97* 609bp, *ccep-135* 1984bp) and 3'UTR (*cep-97* 491bp, *cep-135* 910bp) were amplified from *C. elegans* genomic DNA, coding sequence from cDNA. In the case of CCEP-135, the longest isoform, isoform a, was cloned. All constructs described above were assembled by Gibson assembly [85]. Strains co-expressing endogenously GFP-tagged SPD-5/PLK-1 and GFP nanobody-TurboID expressed under the different tissue-specific promoters, as well strains co-expressing GFP:CCEP-97/ CCEP-135 and TBG-1:mCherry, were constructed by mating. The genotypes of all strains used are listed in the Reagents and Tools Table (Table 1). All strains were maintained at 23°C.

Method details

Sequence analysis and 3D structure predictions. Vertebrate orthologs of uncharacterized proteins in our datasets were identified by reciprocal BLAST analysis using the *C. elegans* protein as the starting point. Where direct comparisons failed to identify a clear homolog, indirect searches were performed using less divergent related species as intermediates. Multiple sequence alignments were generated using MUSCLE within Jalview (<http://www.jalview.org>), while phylogenetic trees were constructed also in Jalview by neighbor joining using the BLOSUM62 matrix. 3D structure predictions of monomeric proteins were obtained from the AlphaFold database [73]. Prediction of homodimeric assemblies of Cep135 homologs was performed with AlphaFold-multimer [86]. Molecular graphics of the structures were created using UCSF ChimeraX [87].

Live imaging. For the experiments presented in S3C and S4C Figs, embryos were dissected in M9, mounted on agarose pads and filmed on a Yokogawa CSU X1 spinning disk confocal mounted on a Zeiss Axio Observer Z1 inverted microscope equipped with a 63x 1.4NA Plan Apochromat objective, 120mW 405nm and 100mW 488nm and 561nm solid-state lasers, 2D-VisiFRAP Galvo FRAP module, Photometrics CoolSNAP-HQ2 cooled CCD and Hamamatsu ImagEM X2 EM-CCD cameras and controlled by VisiView software (Visitron Systems). Images were acquired using the EM-CCD camera with no binning. Image stacks were imported into Fiji for post-acquisition processing, with single planes selected for panel presentation.

Immunofluorescence and fixed imaging. Immunofluorescence experiments were performed as previously described [88] using affinity-purified antibodies to GFP, SPD-5, TAC-1 and HA, as well as fluorescently labeled streptavidin to detect biotinylated proteins. *C. elegans* embryos and L1 larvae were permeabilized by freeze-crack, fixed in -20°C methanol for 20min, rehydrated in PBS, blocked in AbDil (PBS, 2% BSA, 0.1% Triton X-100) for 20min, incubated with 5µg/ml Streptavidin-Alexa Fluor 647 and directly labeled or unlabeled primary antibodies at 1µg/ml in AbDil for 2h (for mouse anti-HA.11 overnight at 4°C), washed 3x in PBST (PBS 0.1% Triton X-100), incubated with secondary antibodies at 7.5µg/ml in AbDil for

Table 1. Reagents and tools table.

Reagent/Resource	Reference or Source	Identifier or Catalog Number
Experimental Models		
<i>C. elegans</i> : Strain DAM280: <i>vieSi13</i> [pAD367; <i>Pccep-97::gfp::ccep-97cDNA::ccep-97 3'UTR</i> ; <i>cb unc-119(+)</i>] II; <i>unc-119(ed3)</i> III	This study	DAM280
<i>C. elegans</i> : Strain DAM1075: <i>spd-5(vie26[gfp::spd-5 +loxP])</i> I	[10]	DAM1075
<i>C. elegans</i> : Strain DAM1210: <i>unc-119(ed3)</i> III; <i>vieSi132</i> [pAD801; <i>Posm-6::TurboID::gfp::spd-5reencoded::spd-5 3'UTR</i> ; <i>cb unc-119(+)</i>] V	This study	DAM1210
<i>C. elegans</i> : Strain DAM1224: <i>vieSi135</i> [pAD773; <i>Pspd-5::gfp::TurboID::spd-5 3'UTR</i> ; <i>cb unc-119(+)</i>] II; <i>unc-119(ed3)</i> III	This study	DAM1224
<i>C. elegans</i> : Strain DAM1235: <i>vieSi145</i> [pAD846; <i>Posm-6::TurboID::gfp::spd-5 3'UTR</i> ; <i>cb unc-119(+)</i>] II; <i>unc-119(ed3)</i> III	This study	DAM1235
<i>C. elegans</i> : Strain DAM1264: <i>vieSi136</i> [pAD847; <i>Pspd-5::gfp::TurboID::spd-5reencoded::spd-5 3'UTR</i> ; <i>cb unc-119(+)</i>] II; <i>unc-119(ed3)</i> III	This study	DAM1264
<i>C. elegans</i> : Strain DAM1281: <i>spd-5(vie26[gfp::spd-5 +loxP])</i> I; <i>vieSi142</i> [pAD861; <i>Ppie-1::vhhGFP4::HA::TurboID::operon-linker::mCherry::his-11::tbb-2 3'UTR</i> ; <i>cb unc-119(+)</i>] II; <i>unc-119(ed3)</i> III?	This study, [45]	DAM1281
<i>C. elegans</i> : Strain DAM1284: <i>vieSi142</i> [pAD861; <i>Ppie-1::vhhGFP4::HA::TurboID::operon-linker::mCherry::his-11::tbb-2 3'UTR</i> ; <i>cb unc-119(+)</i>] II; <i>unc-119(ed3)</i> III	This study	DAM1284
<i>C. elegans</i> : Strain DAM1310: <i>vieSi142</i> [pAD861; <i>Ppie-1::vhhGFP4::HA::TurboID::operon-linker::mCherry::his-11::tbb-2 3'UTR</i> ; <i>cb unc-119(+)</i>] II; <i>plk-1(tl17[plk-1::superfoldergfp +loxP])</i> III	This study, [81]	DAM1310
<i>C. elegans</i> : Strain DAM1312: <i>vieSi147</i> [pAD887; <i>Pnos-2::vhhGFP4::HA::TurboID::nos-2 3'UTR</i> ; <i>cb unc-119(+)</i> ; <i>unc-119(ed3)</i> III	This study	DAM1312
<i>C. elegans</i> : Strain DAM1320: <i>vieSi148</i> [pAD888; <i>Pehn-3a::vhhGFP4::HA::TurboID::ehn-3 3'UTR</i> ; <i>cb unc-119(+)</i> ; <i>unc-119(ed3)</i> III	This study	DAM1320
<i>C. elegans</i> : Strain DAM1321: <i>spd-5(vie26[gfp::spd-5 +loxP])</i> I; <i>vieSi147</i> [pAD887; <i>Pnos-2::vhhGFP4::HA::TurboID::nos-2 3'UTR</i> ; <i>cb unc-119(+)</i>] III; <i>unc-119(ed3)</i> III?	This study, [45]	DAM1321
<i>C. elegans</i> : Strain DAM1327: <i>vieSi152</i> [pAD886; <i>Posm-6::vhhGFP4::HA::TurboID::tbb-2 3'UTR</i> ; <i>cb unc-119(+)</i>] II; <i>unc-119(ed3)</i> III	This study	DAM1327
<i>C. elegans</i> : Strain DAM1329: <i>vieSi154</i> [pAD895; <i>Pplk-1::gfp::TurboID::plk-1::plk-1 3'UTR</i> ; <i>cb unc-119(+)</i>] II; <i>unc-119(ed3)</i> III	This study	DAM1329
<i>C. elegans</i> : Strain DAM1330: <i>vieSi155</i> [pAD896; <i>Pplk-1::gfp::TurboID::plk-1 3'UTR</i> ; <i>cb unc-119(+)</i>] II; <i>unc-119(ed3)</i> III	This study	DAM1330
<i>C. elegans</i> : Strain DAM1333: <i>spd-5(vie26[gfp::spd-5 +loxP])</i> I; <i>vieSi152</i> [pAD886; <i>Posm-6::vhhGFP4::HA::TurboID::tbb-2 3'UTR</i> ; <i>cb unc-119(+)</i>] II; <i>unc-119(ed3)</i> III?	This study, [45]	DAM1333
<i>C. elegans</i> : Strain DAM1335: <i>spd-5(vie26[gfp::spd-5 +loxP])</i> I; <i>vieSi148</i> [pAD888; <i>Pehn-3a::vhhGFP4::HA::TurboID::ehn-3 3'UTR</i> ; <i>cb unc-119(+)</i>] III; <i>unc-119(ed3)</i> III?	This study, [45]	DAM1335
<i>C. elegans</i> : Strain DAM1337: <i>vieSi157</i> [pAD933; <i>Pccep-135::gfp::ccep-135 cDNA::ccep-135 3'UTR</i> ; <i>cb unc-119(+)</i>] II; <i>unc-119(ed3)</i> III	This study	DAM1337
<i>C. elegans</i> : Strain DAM1348: <i>ltSi569</i> [pOD1110; <i>CEOP3608 tbg-1::mCherry</i> ; <i>cb-unc-119(+)</i>] I; <i>vieSi13</i> [pAD367; <i>Pccep-97::gfp::ccep-97 cDNA::ccep-97 3'UTR</i> ; <i>cb unc-119(+)</i>] II; <i>unc-119(ed3)</i> III?	This study, [82]	DAM1348
<i>C. elegans</i> : Strain DAM1349: <i>ltSi569</i> [pOD1110; <i>CEOP3608 tbg-1::mCherry</i> ; <i>cb-unc-119(+)</i>] I; <i>vieSi157</i> [pAD933; <i>Pccep-135::gfp::ccep-135 cDNA::ccep-135 3'UTR</i> ; <i>cb unc-119(+)</i>] II; <i>unc-119(ed3)</i> III?	This study, [82]	DAM1349
<i>C. elegans</i> : Strain EG6249: <i>tTi5605</i> II; <i>unc-119(ed3)</i> III	[26]	EG6249
<i>C. elegans</i> : Strain EG8079: <i>oxTi179</i> II; <i>unc-119(ed3)</i> III	[95]	EG8079
<i>C. elegans</i> : Strain N2: <i>C. elegans</i> wild-type (ancestral)	Caenorhabditis Genetics Center	N2
<i>C. elegans</i> : Strain OD2425: <i>plk-1(tl17[plk-1::superfoldergfp +loxP])</i> III	[81]	OD2425
Recombinant DNA		
Mos Co-injection marker pCFJ104— <i>Pmyo-3::mCherry::unc-54</i>	[26]	Addgene Plasmid # 19328
Mos Co-injection marker pCFJ90— <i>Pmyo-2::mCherry::unc-54utr</i>	[26]	Addgene Plasmid # 19327
Mos Co-injection marker pGH8— <i>pRAB-3::mCherry::unc-54utr</i>	[26]	Addgene Plasmid # 19359

(Continued)

Table 1. (Continued)

Reagent/Resource	Reference or Source	Identifier or Catalog Number
Mos Negative selection marker pMA122—Phsp-16.41::peel-1::tbb-2utr	[96]	Addgene Plasmid # 34873
Mos vector pCFJ151	[26]	Addgene Plasmid # 19330
Antibodies		
Donkey anti-Goat IgG (H+L) Cy2	Jackson ImmunoResearch	Cat# 705-225-147; RRID: AB_2307341
Donkey anti-mouse IgG (H+L) Cy3	Jackson ImmunoResearch	Cat# 715-165-150; RRID: AB_2340813
Goat polyclonal anti-GFP	[39]	N/A
Mouse monoclonal anti-HA.11 (16B12)	Covance	Cat# MMS-101R; RRID: AB_291262
Rabbit polyclonal anti-ceSPD-5	[39]	N/A
Rabbit polyclonal anti-ceTAC-1	[97]	N/A
Oligonucleotides and other sequence-based reagents		
<i>ccep-97(R02F11.4)</i> dsRNA: 1.5mg/ml, amplified from N2 cDNA; forward primer: AATTAACCTCACTAAAGGCAGACGATAAGCTTGGCTGA	This study	AD532
<i>ccep-97</i> reverse primer: TAATACGACTCACTATAGGCTAGCCGATCGTTGATAGCC	This study	AD533
<i>ccep-135(H06I04.1)</i> dsRNA: 2.0mg/ml, amplified from N2 cDNA; forward primer: TAATACGACTCACTATAGGATTCTAAAAATCCCATCAA	This study	AD3144
<i>ccep-135</i> reverse primer: AATTAACCTCACTAAAGGCTGTTCCCTCAACATCTTC	This study	AD3146
<i>spd-5(F56A3.4)</i> dsRNA: 2.3mg/ml, amplified from N2 genomic DNA; forward primer: AATTAACCTCACTAAAGGTGTCGCAACCAGTTCTGAAT	This study	AD548
<i>spd-5</i> reverse primer: TAATACGACTCACTATAGGATGGAGGCAAATTGTTGCTG	This study	AD549
Chemicals, Enzymes and other reagents		
Ammonium bicarbonate	Sigma-Aldrich	Cat# 09830; CAS 1066-33-7
cOmplete Mini EDTA-free Protease Inhibitor Cocktail	Roche	Cat# 11836170001
Dithiothreitol (DTT)	Roche	Cat# 10197777001; CAS# 3483-12-3
Hoechst 33342	Sigma-Aldrich	Cat# B2261; CAS: 875756-97-1
Iodoacetamide	Sigma Aldrich	Cat# I1149-25G; CAS# 144-48-9
Pierce Streptavidin Magnetic Beads	Thermo Fisher Scientific	Cat# S88816
Pierce Sulfo-NHS-Acetate	Thermo Fisher Scientific	Cat# 26777
Streptavidin, Alexa Fluor 647	Thermo Fisher Scientific	Cat# S21374
Trypsin Gold	Promega	Cat# V5280
Vectashield Mounting Medium	Vector Labs	Cat# H-1000
Zeba Spin Desalting Columns, 7K MWCO, 10 mL	Thermo Fisher Scientific	Cat# 89894
Software		
AlphaFold Multimer Colab	[73, 86]	https://colab.research.google.com/github/deepmind/alphafold/blob/main/notebooks/AlphaFold.ipynb
Cassiopeia LFQ	Max Perutz Labs Mass Spectrometry Facility	https://github.com/moritzmadern/Cassiopeia_LFQ
FAIMS MzXML Generator	Coon Group, University of Wisconsin, Madison	https://github.com/coongroup/FAIMS-MzXML-Generator
Fiji v 2.0.0	NIH	https://imagej.net/software/fiji/
GraphPad Prism 6	GraphPad	https://www.graphpad.com/scientific-software/prism/
Jalview v 2.11.1.4	[98]	http://www.jalview.org
MaxQuant v 1.6.17.0	[92]	https://www.maxquant.org
R v 4.0.2	The R Foundation	https://www.r-project.org

<https://doi.org/10.1371/journal.pgen.1010150.t001>

1h followed by Hoechst 33342 at 1 μ g/ml in PBS for 5min, washed in PBST and mounted in Vectashield. 3D widefield datasets were acquired using a 100x 1.4NA Uplan S Apochromat objective on a DeltaVision 2 Ultra microscope equipped with 7-Color SSI module and sCMOS camera and controlled by Acquire Ultra acquisition software (GE Healthcare), computationally deconvolved using the enhanced ratio constrained iterative deconvolution algorithm, and maximum-intensity projected before being imported into Photoshop (Adobe) for panel preparation. No nonlinear gamma corrections were performed during image processing.

Fluorescence recovery after photobleaching. To examine the dynamics of PLK-1 at centrosomes in early embryos, adult worms were dissected in meiosis medium (60% Leibowitz L-15 media, 25mM HEPES pH7.4, 0.5% Inulin, 20% heat-inactivated fetal bovine serum) and embryos filmed without compression [89] on the spinning disk confocal microscope described above. Low laser illumination (max power of 0.32mW) was used to minimize photobleaching. Embryos in the first mitotic division were followed from early prophase, with 6x0.5 μ m z-series acquired using the EM-CCD camera without binning at irregular intervals. Photobleaching was performed in prometaphase using the galvanometer point scanner to target a region encompassing the centrosome with the 405nm laser at 10mW power and embryos imaged until completion of cytokinesis. Embryos were analyzed only if centrosome signal was completely eliminated throughout the entire z-volume.

TurboID-based enzymatic protein labeling and extraction of biotinylated proteins from *C. elegans* embryos. Gravid adult *C. elegans* cultivated in a 500ml liquid culture [90] were bleached to harvest embryos. Embryos were washed 3x with cold M9 followed by 1 wash with lysis buffer H100 (50mM HEPES pH7.4, 1mM EGTA, 1mM MgCl₂, 100mM KCl, 10% Glycerol, 0.05% NP-40) before pelleting at 800g for 2min at 4°C. Embryos were then resuspended with lysis buffer supplemented with Roche cOmplete Mini EDTA-free Protease-Inhibitor-Cocktail (1 tablet/10ml lysis buffer), 1mM PMSF, 1mM Benzamide at a ratio of 1:4 packed embryos to buffer and split into three replicate samples. Embryos in each sample were then lysed by tip sonication (30% continuous output, Bandelin Sonopuls GM70) with three pulses for 15s with brief cooling on ice between pulses. Lysates were clarified by two brief spins at 200g for 3min at 4°C in a benchtop centrifuge before pelleting insoluble cellular material including centrosomes by centrifugation at 20000g for 30min. Pellets were resuspended by boiling in 60 μ l 2% SDS in PBS containing 1% beta-Mercaptoethanol for 30min with multiple vortexing steps in between. 9 volumes of PBS and 1 volume 20% Triton X-100 in PBS were then added and samples sonicated three times for 30s (60% output at 1 pulse/s). Another 9 volumes of PBS were then added and samples sonicated for another 30s as before centrifuging at 20000g for 30min at 4°C and recovering the supernatant. Pierce Streptavidin-coated magnetic beads (150 μ l bead slurry per sample) were equilibrated with PBS containing 0.1% SDS before incubating with solubilized cytoskeletal fractions on a rotator overnight at 4°C. Unbound lysate was then removed and beads washed for 8min each on a rotator at room temperature, first with 2% SDS in ddH₂O, then 0.1% deoxycholic acid, 1% Triton X-100, 1mM EDTA, 500mM NaCl and 50mM HEPES pH7.5, and finally 0.5% deoxycholic acid, 0.5% NP-40, 1mM EDTA, 500mM LiCl and 10mM Tris pH7.5. Beads were then washed 5x for 3min with 50mM Tris pH7.4 before being sent for on-bead protein digestion and mass spectrometry analysis.

TurboID-based enzymatic protein labeling and extraction of biotinylated proteins from *C. elegans* L1 larvae. Gravid adult *C. elegans* cultivated in a 500ml liquid culture [90] were bleached to harvest embryos and those embryos allowed to hatch overnight by shaking in M9 buffer without food at 22°C to obtain a synchronous culture arrested at L1 stage. For the last 2h *E. coli* OP50.1 (800 μ l bacterial slurry/50ml M9) and 1mM biotin were added to stimulate centrosome assembly and biotin incorporation [20]. L1 larvae were then washed three times with ice-cold M9 and allowed to settle on ice after the last wash in order to aspirate off the

supernatant. Two volumes of RIPA buffer (1% Triton X-100, 1mM EDTA, 0.5% sodium deoxycholate, 0.1% SDS, 150mM NaCl, 50mM Tris-HCl pH7.4) supplemented with 1mM PMSF and Roche cOmplete Mini EDTA-free Protease-Inhibitor-Cocktail (1 tablet/25ml lysis buffer) were added to one volume of packed worms. L1 larvae were again allowed to settle on ice and added dropwise to liquid nitrogen to obtain frozen worm 'popcorn', which were ground to a fine powder using a SPEX 6875 cryogenic mill (Settings: 5 cycles, 1min pre-cool, 2min run-time, 1min cool-time; 12 cps) and stored at -80°C. Worm powder was thawed in a 50ml conical tube on a tube roller at 4°C and the sample collected at the bottom of the tube by a brief spin at 200g for 1min at 4°C. SDS and DTT were then added to a final concentration of 1% and 10mM, respectively. Tubes were gently inverted several times and the sample split into three 2ml microcentrifuge tubes which were immediately incubated at 90°C for 5min. After boiling, samples were sonicated by tip sonication (20% continuous output, Bandelin Sonopuls GM70) with 2 pulses of 1min with brief cooling between pulses. Samples were then adjusted to 2M urea using a stock solution of 8M urea, 1% SDS, 50mM Tris-HCl pH7.4, 150mM NaCl) and centrifuged at 100000g for 45min at 22°C. The clear supernatant between pellet and surface lipid layer was transferred to a new tube. Zeba spin desalting columns (7K MWCO) (ThermoFisher) were equilibrated three times with 5ml RIPA buffer containing 1% SDS, 2M urea and protease inhibitors as above by centrifugation at 1000g for 5min. In order to remove free biotin, clarified samples were loaded twice onto equilibrated columns and desalted by centrifugation (1000g, 5min) to remove free biotin.

Pierce Streptavidin magnetic beads (150µl bead slurry per sample) were equilibrated with 50mM HEPES-NaOH pH7.8 containing 0.2% Tween-20 by washing them three times with the buffer. A mixture of 190µl 50mM HEPES-NaOH pH7.8 containing 0.2% Tween-20 and 10µl 100mM Pierce Sulfo-NHS-Acetate (dissolved in DMSO) was used to acetylate free amines on streptavidin beads by incubation at room temperature for 1h (see also <https://dx.doi.org/10.17504/protocols.io.b3sqndw>). Beads were then washed three times with 50mM NH₄HCO₃ containing 0.2% Tween-20 before adding the desalted and clarified sample solution and incubating on a rotator overnight at room temperature. Following incubation, unbound lysate was removed and beads washed twice with 150mM NaCl, 1mM EDTA, 2% SDS, 50mM Tris-HCl, pH7.4, once with 1X TBS pH7.4, twice with 1M KCl, 1mM EDTA, 50mM Tris-HCl, 0.1% Tween-20, pH7.4, twice with 0.1M Na₂CO₃, 0.1% Tween-20, pH11.5, twice with 2M urea, 10mM Tris-HCl, 0.1% Tween-20, pH8.0 and finally five times with 1X TBS. Beads were then resuspended in 1X TBS buffer and sent for on-bead protein digestion and mass spectrometry analysis.

Sample preparation for mass spectrometry analysis. Beads were resuspended in 50µl 1M urea and 50mM ammonium bicarbonate. Disulfide bonds were reduced with 2µl of 250mM dithiothreitol (DTT) for 30min at room temperature before adding 2µl of 500mM iodoacetamide and incubating for 30min at room temperature in the dark. Remaining iodoacetamide was quenched with 1µl of 250mM DTT for 10min. Proteins were digested with 300ng trypsin (Trypsin Gold, Promega) in 3µl 50mM ammonium bicarbonate followed by incubation at 37°C overnight. The supernatant without beads was transferred to a new tube, the digest stopped by addition of trifluoroacetic acid (TFA) to a final concentration of 0.5% and the peptides desalted using C18 Stagetips [91].

Liquid chromatography separation coupled to mass spectrometry. Peptides were separated on an Ultimate 3000 RSLC nano-flow chromatography system (Thermo-Fisher), using a pre-column for sample loading (Acclaim PepMap C18, 2cm × 0.1mm, 5µm, Thermo-Fisher), and a C18 analytical column (Acclaim PepMap C18, 50cm × 0.75mm, 2µm, Thermo-Fisher), applying a segmented linear gradient from 2% to 35% and finally 80% solvent B (80% acetonitrile, 0.1% formic acid; solvent A 0.1% formic acid) at a flow rate of 230nL/min over 120min.

The peptides eluted from the nano-LC were analyzed by mass spectrometry as described below.

For SPD-5 embryo samples, a Q Exactive HF-X Orbitrap mass spectrometer (Thermo Fisher) coupled to the column with a nano-spray ion-source using coated emitter tips (PepSep, MSWil), was used with the following settings: The mass spectrometer was operated in data-dependent acquisition mode (DDA), survey scans were obtained in a mass range of 375-1500m/z with lock mass activated, at a resolution of 120k at 200m/z and an AGC target value of 3E6. The 12 most intense ions were selected with an isolation width of 1.4m/z, fragmented in the HCD cell at 28% collision energy and the spectra recorded for max. 200ms at a target value of 1E5 and a resolution of 30k. Peptides with a charge of +2 to +6 were included for fragmentation, the peptide match and the exclude isotopes features enabled, and selected precursors were dynamically excluded from repeated sampling for 30s. Raw data were directly used for further analysis.

For all other samples, an Exploris 480 Orbitrap mass spectrometer (Thermo Fisher) coupled to the column with a FAIMS pro ion-source (Thermo-Fisher) using coated emitter tips (PepSep, MSWil), was used with the following settings: The mass spectrometer was operated in DDA mode with two FAIMS compensation voltages (CV) set to -45 or -60 and 1.5s cycle time per CV. The survey scans were obtained in a mass range of 350-1200m/z, at a resolution of 60k at 200m/z and a normalized AGC target at 100%. The most intense ions were selected with an isolation width of 1.0m/z, fragmented in the HCD cell at 28% collision energy and the spectra recorded for max. 100ms at a normalized AGC target of 100% and a resolution of 15k. Peptides with a charge of +2 to +6 were included for fragmentation, the peptide match feature was set to preferred, the exclude isotope feature was enabled, and selected precursors were dynamically excluded from repeated sampling for 45s. Raw data were split for each CV and converted to mxml-format using freely available software (<https://github.com/coongroup/FAIMS-MzXML-Generator>) for further analysis.

Quantification and statistical analysis

Image analysis. Quantification of centrosomal PLK-1 signal was performed in Fiji. GFP signal was measured on single planes at each time point. Two variable size concentric regions were drawn around the centrosome, a smaller one encompassing the centrosome and a larger one including the surrounding cytoplasm as background. The integrated GFP intensity was then calculated by subtracting the mean fluorescence intensity in the area between the two boxes (mean background) from the mean intensity in the smaller box and multiplying by the area of the smaller box. Measurements taken after photobleaching were normalized to the mean intensity of measurements shortly before photobleaching. GraphPad Prism was then used to fit the data to the exponential equation $Y = A * (1 - \exp(-k * X)) + B$ where A is the mobile fraction, B is the background left after the bleach, and the half life $t_{1/2} = \ln(0.5) / -k$. R^2 values are the correlation coefficient obtained by fitting experimental data to the model. Data points on the graphs are the mean of the normalized GFP intensity measurements.

Mass spectrometry database search and analysis. MS data were analyzed using the MaxQuant software package [92] and the Uniprot *Caenorhabditis elegans* reference proteome (www.uniprot.org), as well as a database of most common contaminants. The search was performed with full trypsin specificity and a maximum of two missed cleavages at a protein and peptide spectrum match false discovery rate of 1%. Carbamidomethylation of cysteine residues were set as fixed, oxidation of methionine and N-terminal acetylation as variable modifications. For label-free quantification the “match between runs” feature and the LFQ normalization function were activated—all other parameters were left at default. MaxQuant output tables were further processed in R (The R Foundation) using a script developed in-house

(https://github.com/moritzmadern/Cassiopia_LFQ). Reverse database identifications, contaminant proteins, protein groups identified only by a modified peptide, protein groups with less than two quantitative values in one experimental group, and protein groups with less than 2 razor peptides were removed from further analysis.

The analysis of differential abundance in mass spectrometry-based proteomics data sets requires the application of missing value imputation where a particular protein of interest is missing in one or more replicates [93]. For the data presented in the figures we decided to perform deterministic lowest of detection (LOD) within Microsoft Excel for the comparison of different runs of mass spectrometry. LOD uses the lowest measured LFQ value within a run to fill in missing LFQ values after filtering out contaminants and proteins with less than two razor and unique peptides [94]. A common alternative approach presented in the Supplemental tables (S1 and S2 Tables) is random drawing from a left-censored normal distribution (ND) in logarithmic space, which we performed in R. For this, missing values were replaced by randomly drawing data points from a normal distribution modeled on the whole dataset (data mean shifted by -1.8 standard deviations, width of distribution of 0.3 standard deviations). While the latter approach is often appropriate when comparing e.g. two treatment conditions, in our case we noted that centrosomal proteins frequently were absent in one or all control samples but also not highly abundant in the experimental samples, likely because of their restricted spatial distribution and low abundance within the cell. Application of ND imputation consequently led to misleading variations in protein abundance with less clear separation of likely proximity interactors from apparent contaminants, while also frequently inverting sample enrichment ratios between hits. In contrast, we found LOD resulted in a more accurate representation of sample enrichment and this approach was used in our data presentations. In essentially all cases, however, likely proximity interactors passed the significance threshold with both methods of imputation. These were defined as a log₂ fold change of >1 and a p-value in an unpaired t-test of <0.05. GraphPad Prism was used to prepare bar graphs, volcano and MA plots using LFQ values imported from Microsoft Excel.

Supporting information

S1 Fig. The GFP nanobody:TurboID tag. (A) Schematic of the indirect TurboID construct developed in this study. A GFP nanobody:HA:TurboID cassette is expressed under a ubiquitous or tissue/cell-specific promoter and 3' regulatory sequences. The vector backbone is based on pCFJ151 for Mos1 transposon-mediated integration at a defined chromosomal locus [26], sites for which have been established on all five autosomes in *C. elegans* [95]. (B) DNA sequence of the GFP nanobody:HA:TurboID cassette and conceptual translation. (C) Promoters for ubiquitous, tissue/cell-specific and inducible expression in *C. elegans*, selected for the low expression required for TurboID. Promoters in bold have been used and validated in this study. For inducible expression, a strategy such as using FLP-recombinase under the control of the *Phsp-16.48* heat shock promoter to excise a repressive "off-element" [99] avoids the variability and overexpression associated with the use of the heat-shock promoter alone and additionally confers the potential for tissue-specific inducible expression not explored in this study. (TIF)

S2 Fig. Tissue-specific labeling using direct TurboID and further data on TurboID experiments. (A) Direct TurboID applied to SPD-5 in ciliated neurons. Immunofluorescence micrograph of head of L1 larva from strain expressing TurboID:GFP:SPD-5 under the ciliated neuron-specific promoter *osm-6* stained for GFP, biotin (streptavidin) and TAC-1 as a PCM countermarker. Biotinylation signal is observed at the ciliary base coincident with GFP:SPD-5/TAC-1 signal. (B) Result of LC-MS/MS analysis for direct TurboID on SPD-5 in ciliated

neurons. Volcano plot of $-\log_{10}$ p-values against \log_2 fold change (sample/control). Significantly enriched proteins (\log_2 enrichment >1 , p-value <0.05) are indicated in pink, with selected proteins highlighted. Comparison with indirect TurboID presented in Fig 3C. See also S1 Table. (C-H) Volcano plots of average \log_2 LFQ intensity (sample) against \log_2 fold change (sample/control) for direct (C, D) and indirect (E, F) TurboID on SPD-5 and PLK-1 in embryos, direct TurboID on SPD-5 in ciliated neurons (G) and indirect TurboID on SPD-5 in germ cell precursors (H). Significantly enriched proteins (\log_2 enrichment >1 , p-value <0.05) are indicated in pink, with selected proximity interactors highlighted. Note that interactors are present at much lower levels in the sample compared to endogenously biotinylated proteins, highlighting the importance of proper sample normalization. Scale bar in A is $10\mu\text{m}$. (TIF)

S3 Fig. R02F11.4/CCEP-97 as a putative ortholog of Cep97. (A, B) Multiple sequence alignment (A) and neighbor joining phylogenetic tree (B) of selected Cep97 orthologs. Accession numbers are provided in S2 Table. Note that tree largely reflects pattern of evolutionary divergence. (C) Endogenous promoter GFP fusion of CCEP-97 does not localize to the mitotic centrosome in the early embryo or the non-centrosomal microtubule-organizing center in the intestinal primordium of bean-stage embryos ($\sim 360\text{min}$ after fertilization), both marked by TBG-1:mCherry. GFP images scaled to centrosomal signal at germ cell precursors in L1 stage larvae. Scale bar in C is $10\mu\text{m}$. (TIF)

S4 Fig. H06I04.1/CCEP-135 as a putative ortholog of Cep135/BLD10. (A, B) Multiple sequence alignment (A) and neighbor joining phylogenetic tree (B) of selected Cep135 orthologs. Accession numbers are provided in S2 Table. Note that tree largely reflects pattern of evolutionary divergence. (C) Endogenous promoter GFP fusion of CCEP-135 does not localize to the mitotic centrosome in the early embryo or the non-centrosomal microtubule-organizing center in the intestinal primordium of bean-stage embryos ($\sim 360\text{min}$ after fertilization), both marked by TBG-1:mCherry. GFP images scaled to centrosomal signal at ciliary base in L1 stage larvae. Scale bar in C is $10\mu\text{m}$. (TIF)

S1 Table. Mass spectrometry data. Complete list of proteins identified by mass spectrometry in each direct/indirect TurboID run, including corresponding controls. Only the most relevant data rows and columns are displayed by default. The full processed MS data including excluded peptide groups, spectral counts and differential abundance analysis using missing value imputation by random drawing from a left-censored normal distribution (ND) can be found by expanding the collapsed rows and columns. In addition, the raw proteomics data have been deposited to the ProteomeXchange Consortium via the PRIDE partner repository (<http://www.ebi.ac.uk/pride>, [100]) with the dataset identifier PXD031970. (XLSX)

S2 Table. List of Cep97/Cep135 orthologs. GenBank accession numbers for Cep97/Cep135 orthologs presented in Figs 4, S3 and S4. (XLSX)

Acknowledgments

We thank members of the Campbell and Dammermann labs for discussions, the *Caenorhabditis* Genetics Center, Luisa Cochella, Jessica Feldman and Karen Oegema for strains and reagents, Brooke Morriswood and Mario de Bono for sharing protocols and Markus Hartl,

Natascha Hartl and Weiqiang Chen of the Max Perutz Labs Mass Spectrometry facility and Josef Gotzmann and Thomas Peterbauer of the BioOptics facility for technical assistance.

Author Contributions

Conceptualization: Elisabeth Holzer, Cornelia Rumpf-Kienzl, Alexander Dammermann.

Data curation: Elisabeth Holzer, Cornelia Rumpf-Kienzl, Sebastian Falk, Alexander Dammermann.

Formal analysis: Elisabeth Holzer, Cornelia Rumpf-Kienzl, Sebastian Falk, Alexander Dammermann.

Funding acquisition: Alexander Dammermann.

Investigation: Elisabeth Holzer, Cornelia Rumpf-Kienzl, Alexander Dammermann.

Methodology: Elisabeth Holzer, Cornelia Rumpf-Kienzl, Alexander Dammermann.

Project administration: Alexander Dammermann.

Supervision: Alexander Dammermann.

Validation: Elisabeth Holzer, Cornelia Rumpf-Kienzl, Alexander Dammermann.

Visualization: Elisabeth Holzer, Sebastian Falk, Alexander Dammermann.

Writing – original draft: Elisabeth Holzer, Alexander Dammermann.

Writing – review & editing: Elisabeth Holzer, Cornelia Rumpf-Kienzl, Sebastian Falk, Alexander Dammermann.

References

1. Oegema K, Hyman AA. Cell division. WormBook. 2006:1–40. Epub 2007/12/01. <https://doi.org/10.1895/wormbook.1.72.1> PMID: 18050484; PubMed Central PMCID: PMC4780891.
2. Pintard L, Bowerman B. Mitotic Cell Division in *Caenorhabditis elegans*. Genetics. 2019; 211(1):35–73. Epub 2019/01/11. <https://doi.org/10.1534/genetics.118.301367> PMID: 30626640; PubMed Central PMCID: PMC6325691.
3. Kitagawa D, Vakonakis I, Olieric N, Hilbert M, Keller D, Olieric V, et al. Structural basis of the 9-fold symmetry of centrioles. Cell. 2011; 144(3):364–75. <https://doi.org/10.1016/j.cell.2011.01.008> PMID: 21277013.
4. van Breugel M, Hirono M, Andreeva A, Yanagisawa HA, Yamaguchi S, Nakazawa Y, et al. Structures of SAS-6 suggest its organization in centrioles. Science. 2011; 331(6021):1196–9. <https://doi.org/10.1126/science.1199325> PMID: 21273447.
5. Woodruff JB, Ferreira Gomes B, Widlund PO, Mahamid J, Honigsmann A, Hyman AA. The Centrosome Is a Selective Condensate that Nucleates Microtubules by Concentrating Tubulin. Cell. 2017; 169(6):1066–77.e10. Epub 2017/06/03. <https://doi.org/10.1016/j.cell.2017.05.028> PMID: 28575670.
6. Woodruff JB, Wueseke O, Viscardi V, Mahamid J, Ochoa SD, Bunkenborg J, et al. Centrosomes. Regulated assembly of a supramolecular centrosome scaffold in vitro. Science. 2015; 348(6236):808–12. Epub 2015/05/16. <https://doi.org/10.1126/science.aaa3923> PMID: 25977552.
7. Erpf AC, Stenzel L, Memar N, Antoniolli M, Osepashvili M, Schnabel R, et al. PCMD-1 Organizes Centrosome Matrix Assembly in *C. elegans*. Curr Biol. 2019; 29(8):1324–36.e6. Epub 2019/04/16. <https://doi.org/10.1016/j.cub.2019.03.029> PMID: 30982652.
8. Sugioka K, Hamill DR, Lowry JB, McNeely ME, Enrick M, Richter AC, et al. Centriolar SAS-7 acts upstream of SPD-2 to regulate centriole assembly and pericentriolar material formation. eLife. 2017;6. Epub 2017/01/17. <https://doi.org/10.7554/eLife.20353> PMID: 28092264; PubMed Central PMCID: PMC5342823.
9. von Tobel L, Mikeladze-Dvali T, Delattre M, Balestra FR, Blanchoud S, Finger S, et al. SAS-1 is a C2 domain protein critical for centriole integrity in *C. elegans*. PLoS Genet. 2014; 10(11):e1004777. Epub 2014/11/21. <https://doi.org/10.1371/journal.pgen.1004777> PMID: 25412110; PubMed Central PMCID: PMC4238951.

10. Garbrecht J, Laos T, Holzer E, Dillinger M, Dammermann A. An acentriolar centrosome at the *C. elegans* ciliary base. *Curr Biol*. 2021; 31(11):2418–28.e8. Epub 2021/04/03. <https://doi.org/10.1016/j.cub.2021.03.023> PMID: 33798427.
11. Magescas J, Eskinazi S, Tran MV, Feldman JL. Centriole-less pericentriolar material serves as a microtubule organizing center at the base of *C. elegans* sensory cilia. *Curr Biol*. 2021; 31(11):2410–7.e6. Epub 2021/04/03. <https://doi.org/10.1016/j.cub.2021.03.022> PMID: 33798428; PubMed Central PMCID: PMC8277230.
12. Feldman JL, Priess JR. A role for the centrosome and PAR-3 in the hand-off of MTOC function during epithelial polarization. *Curr Biol*. 2012; 22(7):575–82. Epub 2012/03/20. <https://doi.org/10.1016/j.cub.2012.02.044> PMID: 22425160; PubMed Central PMCID: PMC3409831.
13. Sanchez AD, Branon TC, Cote LE, Papagiannakis A, Liang X, Pickett MA, et al. Proximity labeling reveals non-centrosomal microtubule-organizing center components required for microtubule growth and localization. *Curr Biol*. 2021; 31(16):3586–600.e11. Epub 20210708. <https://doi.org/10.1016/j.cub.2021.06.021> PMID: 34242576; PubMed Central PMCID: PMC8478408.
14. Wueseke O, Bunkenborg J, Hein MY, Zinke A, Viscardi V, Woodruff JB, et al. The *Caenorhabditis elegans* pericentriolar material components SPD-2 and SPD-5 are monomeric in the cytoplasm before incorporation into the PCM matrix. *Mol Biol Cell*. 2014; 25(19):2984–92. Epub 2014/08/12. <https://doi.org/10.1091/mbc.E13-09-0514> PMID: 25103243; PubMed Central PMCID: PMC4230587.
15. Roux KJ, Kim DI, Raida M, Burke B. A promiscuous biotin ligase fusion protein identifies proximal and interacting proteins in mammalian cells. *J Cell Biol*. 2012; 196(6):801–10. Epub 2012/03/14. <https://doi.org/10.1083/jcb.201112098> [pii] PMID: 22412018; PubMed Central PMCID: PMC3308701.
16. Firat-Karalar EN, Rauniyar N, Yates JR 3rd, Stearns T. Proximity interactions among centrosome components identify regulators of centriole duplication. *Curr Biol*. 2014; 24(6):664–70. Epub 2014/03/13. <https://doi.org/10.1016/j.cub.2014.01.067> PMID: 24613305; PubMed Central PMCID: PMC4004176.
17. Gheiratmand L, Coyaud E, Gupta GD, Laurent EM, Hasegan M, Prosser SL, et al. Spatial and proteomic profiling reveals centrosome-independent features of centriolar satellites. *Embo j*. 2019; 38(14):e101109. Epub 2019/07/16. <https://doi.org/10.15252/embj.2018101109> PMID: 31304627; PubMed Central PMCID: PMC6627244.
18. Gupta Gagan D, Coyaud É, Gonçalves J, Mojarad Bahareh A, Liu Y, Wu Q, et al. A Dynamic Protein Interaction Landscape of the Human Centrosome-Cilium Interface. *Cell*. 2015; 163(6):1484–99. <https://doi.org/10.1016/j.cell.2015.10.065> PMID: 26638075
19. Branon TC, Bosch JA, Sanchez AD, Udeshi ND, Svinkina T, Carr SA, et al. Efficient proximity labeling in living cells and organisms with TurboID. *Nat Biotechnol*. 2018; 36(9):880–7. Epub 2018/08/21. <https://doi.org/10.1038/nbt.4201> PMID: 30125270; PubMed Central PMCID: PMC6126969.
20. Artan M, Barratt S, Flynn SM, Begum F, Skehel M, Nicolas A, et al. Interactome analysis of *C. elegans* synapses by TurboID-based proximity labeling. *J Biol Chem*. 2021:101094. Epub 2021/08/21. <https://doi.org/10.1016/j.jbc.2021.101094> PMID: 34416233.
21. Hamill DR, Severson AF, Carter JC, Bowerman B. Centrosome maturation and mitotic spindle assembly in *C. elegans* require SPD-5, a protein with multiple coiled-coil domains. *Dev Cell*. 2002; 3(5):673–84. [https://doi.org/10.1016/s1534-5807\(02\)00327-1](https://doi.org/10.1016/s1534-5807(02)00327-1) PMID: 12431374.
22. Laos T, Cabral G, Dammermann A. Isotropic incorporation of SPD-5 underlies centrosome assembly in *C. elegans*. *Curr Biol*. 2015; 25(15):R648–R9. <https://doi.org/10.1016/j.cub.2015.05.060> PMID: 26241136
23. Cheeseman IM, Desai A. A combined approach for the localization and tandem affinity purification of protein complexes from metazoans. *Sci STKE*. 2005; 2005(266):pl1. <https://doi.org/10.1126/stke.2662005pl1> PMID: 15644491.
24. Kishi K, van Vugt MA, Okamoto K, Hayashi Y, Yaffe MB. Functional dynamics of Polo-like kinase 1 at the centrosome. *Mol Cell Biol*. 2009; 29(11):3134–50. Epub 2009/03/25. <https://doi.org/10.1128/MCB.01663-08> PMID: 19307309; PubMed Central PMCID: PMC2682011.
25. Mahen R, Jeyasekharan AD, Barry NP, Venkitaraman AR. Continuous polo-like kinase 1 activity regulates diffusion to maintain centrosome self-organization during mitosis. *Proc Natl Acad Sci U S A*. 2011; 108(22):9310–5. Epub 2011/05/18. <https://doi.org/10.1073/pnas.1101112108> PMID: 21576470; PubMed Central PMCID: PMC3107272.
26. Frokjaer-Jensen C, Davis MW, Hopkins CE, Newman BJ, Thummel JM, Olesen SP, et al. Single-copy insertion of transgenes in *Caenorhabditis elegans*. *Nat Genet*. 2008; 40(11):1375–83. <https://doi.org/10.1038/ng.248> PMID: 18953339.
27. Schlaitz AL, Srayko M, Dammermann A, Quintin S, Wielsch N, MacLeod I, et al. The *C. elegans* RSA complex localizes protein phosphatase 2A to centrosomes and regulates mitotic spindle assembly. *Cell*. 2007; 128(1):115–27. <https://doi.org/10.1016/j.cell.2006.10.050> PMID: 17218259.

28. Kemp CA, Kopish KR, Zipperlen P, Ahringer J, O'Connell KF. Centrosome Maturation and Duplication in *C. elegans* Require the Coiled-Coil Protein SPD-2. *Dev Cell*. 2004; 6(4):511–23. [https://doi.org/10.1016/s1534-5807\(04\)00066-8](https://doi.org/10.1016/s1534-5807(04)00066-8) PMID: 15068791.
29. Pelletier L, Özlü N, Hannak E, Cowan C, Habermann B, Ruer M, et al. The *Caenorhabditis elegans* Centrosomal Protein SPD-2 Is Required for both Pericentriolar Material Recruitment and Centriole Duplication. *Curr Biol*. 2004; 14:863–73. <https://doi.org/10.1016/j.cub.2004.04.012> PMID: 15186742
30. Bauer M, Cubizolles F, Schmidt A, Nigg EA. Quantitative analysis of human centrosome architecture by targeted proteomics and fluorescence imaging. *Embo j*. 2016; 35(19):2152–66. Epub 2016/08/20. <https://doi.org/10.15252/embj.201694462> PMID: 27539480; PubMed Central PMCID: PMC5048348.
31. Kim DI, Birendra KC, Zhu W, Motamedchaboki K, Doye V, Roux KJ. Probing nuclear pore complex architecture with proximity-dependent biotinylation. *Proc Natl Acad Sci U S A*. 2014; 111(24):E2453–61. Epub 2014/06/14. <https://doi.org/10.1073/pnas.1406459111> PMID: 24927568; PubMed Central PMCID: PMC4066523.
32. Espiritu EB, Krueger LE, Ye A, Rose LS. CLASPs function redundantly to regulate astral microtubules in the *C. elegans* embryo. *Dev Biol*. 2012; 368(2):242–54. Epub 2012/05/23. <https://doi.org/10.1016/j.ydbio.2012.05.016> PMID: 22613359; PubMed Central PMCID: PMC3600381.
33. Swan KA, Severson AF, Carter JC, Martin PR, Schnabel H, Schnabel R, et al. *cyk-1*: a *C. elegans* FH gene required for a late step in embryonic cytokinesis. *J Cell Sci*. 1998; 111 (Pt 14):2017–27. Epub 1998/07/01. PubMed PMID: 9645949.
34. Diogon M, Wissler F, Quintin S, Nagamatsu Y, Sookhareea S, Landmann F, et al. The RhoGAP RGA-2 and LET-502/ROCK achieve a balance of actomyosin-dependent forces in *C. elegans* epidermis to control morphogenesis. *Development*. 2007; 134(13):2469–79. Epub 2007/06/01. <https://doi.org/10.1242/dev.005074> PMID: 17537791.
35. Mizumoto K, Sawa H. Cortical beta-catenin and APC regulate asymmetric nuclear beta-catenin localization during asymmetric cell division in *C. elegans*. *Dev Cell*. 2007; 12(2):287–99. Epub 2007/02/06. <https://doi.org/10.1016/j.devcel.2007.01.004> PMID: 17276345.
36. Boxem M, Maliga Z, Klitgord N, Li N, Lemmens I, Mana M, et al. A protein domain-based interactome network for *C. elegans* early embryogenesis. *Cell*. 2008; 134(3):534–45. <https://doi.org/10.1016/j.cell.2008.07.009> PMID: 18692475.
37. Zhong W, Sternberg PW. Genome-wide prediction of *C. elegans* genetic interactions. *Science*. 2006; 311(5766):1481–4. Epub 2006/03/11. <https://doi.org/10.1126/science.1123287> PMID: 16527984.
38. Tavernier N, Noatynska A, Panbianco C, Martino L, Van Hove L, Schwager F, et al. Cdk1 phosphorylates SPAT-1/Bora to trigger PLK-1 activation and drive mitotic entry in *C. elegans* embryos. *J Cell Biol*. 2015; 208(6):661–9. Epub 2015/03/11. <https://doi.org/10.1083/jcb.201408064> PMID: 25753036; PubMed Central PMCID: PMC4362466.
39. Dammermann A, Muller-Reichert T, Pelletier L, Habermann B, Desai A, Oegema K. Centriole assembly requires both centriolar and pericentriolar material proteins. *Dev Cell*. 2004; 7(6):815–29. <https://doi.org/10.1016/j.devcel.2004.10.015> PMID: 15572125.
40. Dammermann A, Pemble H, Mitchell BJ, McLeod I, Yates JR, 3rd, Kintner C, et al. The hydrolethalus syndrome protein HYLS-1 links core centriole structure to cilia formation. *Genes Dev*. 2009; 23(17):2046–59. <https://doi.org/10.1101/gad.1810409> PMID: 19656802.
41. Rothbauer U, Zolghadr K, Tillib S, Nowak D, Schermelleh L, Gahl A, et al. Targeting and tracing antigens in live cells with fluorescent nanobodies. *Nat Methods*. 2006; 3(11):887–9. Epub 2006/10/25. <https://doi.org/10.1038/nmeth953> PMID: 17060912.
42. Xiong Z, Lo HP, McMahon KA, Martel N, Jones A, Hill MM, et al. In vivo proteomic mapping through GFP-directed proximity-dependent biotin labelling in zebrafish. *eLife*. 2021;10. Epub 2021/02/17. <https://doi.org/10.7554/eLife.64631> PMID: 33591275; PubMed Central PMCID: PMC7906605.
43. Piano F, Schetter AJ, Morton DG, Gunsalus KC, Reinke V, Kim SK, et al. Gene clustering based on RNAi phenotypes of ovary-enriched genes in *C. elegans*. *Curr Biol*. 2002; 12(22):1959–64. [https://doi.org/10.1016/s0960-9822\(02\)01301-5](https://doi.org/10.1016/s0960-9822(02)01301-5) PMID: 12445391.
44. Ramani A, Mariappan A, Gottardo M, Mandad S, Urlaub H, Avidor-Reiss T, et al. Plk1/Polo Phosphorylates Sas-4 at the Onset of Mitosis for an Efficient Recruitment of Pericentriolar Material to Centrosomes. *Cell reports*. 2018; 25(13):3618–30.e6. Epub 2018/12/28. <https://doi.org/10.1016/j.celrep.2018.11.102> PMID: 30590037.
45. Cabral G, Laos T, Dumont J, Dammermann A. Differential Requirements for Centrioles in Mitotic Centrosome Growth and Maintenance. *Dev Cell*. 2019; 50(3):355–66.e6. Epub 2019/07/16. <https://doi.org/10.1016/j.devcel.2019.06.004> PMID: 31303441.
46. Joukov V, De Nicolo A, Rodriguez A, Walter JC, Livingston DM. Centrosomal protein of 192 kDa (Cep192) promotes centrosome-driven spindle assembly by engaging in organelle-specific Aurora A

- activation. *Proc Natl Acad Sci U S A*. 2010; 107(49):21022–7. Epub 2010/11/26. <https://doi.org/10.1073/pnas.1014664107> PMID: 21097701; PubMed Central PMCID: PMC3000277.
47. Joukov V, Walter JC, De Nicolo A. The Cep192-organized aurora A-Plk1 cascade is essential for centrosome cycle and bipolar spindle assembly. *Mol Cell*. 2014; 55(4):578–91. Epub 2014/07/22. <https://doi.org/10.1016/j.molcel.2014.06.016> PMID: 25042804; PubMed Central PMCID: PMC4245277.
 48. Heiman MG, Shaham S. DEX-1 and DYF-7 establish sensory dendrite length by anchoring dendritic tips during cell migration. *Cell*. 2009; 137(2):344–55. Epub 2009/04/07. <https://doi.org/10.1016/j.cell.2009.01.057> PMID: 19344940; PubMed Central PMCID: PMC2673108.
 49. Inglis PN, Ou G, Leroux MR, Scholey JM. The sensory cilia of *Caenorhabditis elegans*. *WormBook*. 2007:1–22. Epub 2007/12/01. <https://doi.org/10.1895/wormbook.1.126.2> PMID: 18050505.
 50. Sulston JE, Horvitz HR. Post-embryonic cell lineages of the nematode, *Caenorhabditis elegans*. *Dev Biol*. 1977; 56(1):110–56. Epub 1977/03/01. [https://doi.org/10.1016/0012-1606\(77\)90158-0](https://doi.org/10.1016/0012-1606(77)90158-0) PMID: 838129
 51. Serwas D, Su TY, Roessler M, Wang S, Dammermann A. Centrioles initiate cilia assembly but are dispensable for maturation and maintenance in *C. elegans*. *J Cell Biol*. 2017; 216(6):1659–71. Epub 2017/04/16. <https://doi.org/10.1083/jcb.201610070> PMID: 28411189; PubMed Central PMCID: PMC5461022.
 52. Johnson TE, Mitchell DH, Kline S, Kemal R, Foy J. Arresting development arrests aging in the nematode *Caenorhabditis elegans*. *Mechanisms of Ageing and Development*. 1984; 28(1):23–40. [https://doi.org/10.1016/0047-6374\(84\)90150-7](https://doi.org/10.1016/0047-6374(84)90150-7) PMID: 6542614
 53. Mohan S, Timbers TA, Kennedy J, Blacque OE, Leroux MR. Striated rootlet and nonfilamentous forms of rootletin maintain ciliary function. *Curr Biol*. 2013; 23(20):2016–22. Epub 2013/10/08. <https://doi.org/10.1016/j.cub.2013.08.033> PMID: 24094853.
 54. Zach F, Grassmann F, Langmann T, Sorusch N, Wolfrum U, Stöhr H. The retinitis pigmentosa 28 protein FAM161A is a novel ciliary protein involved in intermolecular protein interaction and microtubule association. *Hum Mol Genet*. 2012; 21(21):4573–86. Epub 2012/07/14. <https://doi.org/10.1093/hmg/dds268> PMID: 22791751.
 55. Jensen VL, Carter S, Sanders AA, Li C, Kennedy J, Timbers TA, et al. Whole-Organism Developmental Expression Profiling Identifies RAB-28 as a Novel Ciliary GTPase Associated with the BBSome and Intraflagellar Transport. *PLoS Genet*. 2016; 12(12):e1006469. Epub 20161208. <https://doi.org/10.1371/journal.pgen.1006469> PMID: 27930654; PubMed Central PMCID: PMC5145144.
 56. Casenghi M, Meraldi P, Weinhart U, Duncan PI, Korner R, Nigg EA. Polo-like Kinase 1 Regulates Nlp, a Centrosome Protein Involved in Microtubule Nucleation. *Dev Cell*. 2003; 5(1):113–25. [https://doi.org/10.1016/s1534-5807\(03\)00193-x](https://doi.org/10.1016/s1534-5807(03)00193-x) PMID: 12852856.
 57. Di Gioia SA, Letteboer SJ, Kostic C, Bandah-Rozenfeld D, Hettterschijt L, Sharon D, et al. FAM161A, associated with retinitis pigmentosa, is a component of the cilia-basal body complex and interacts with proteins involved in ciliopathies. *Hum Mol Genet*. 2012; 21(23):5174–84. Epub 2012/09/04. <https://doi.org/10.1093/hmg/dds368> PMID: 22940612.
 58. Le Guennec M, Kléna N, Gambarotto D, Laporte MH, Tassin AM, van den Hoek H, et al. A helical inner scaffold provides a structural basis for centriole cohesion. *Science advances*. 2020; 6(7):eaaz4137. Epub 2020/02/29. <https://doi.org/10.1126/sciadv.aaz4137> PMID: 32110738; PubMed Central PMCID: PMC7021493.
 59. Ganier O, Schnerch D, Oertle P, Lim RY, Plodinec M, Nigg EA. Structural centrosome aberrations promote non-cell-autonomous invasiveness. *Embo j*. 2018; 37(9). Epub 2018/03/24. <https://doi.org/10.15252/emj.201798576> PMID: 29567643; PubMed Central PMCID: PMC5920242.
 60. Fukuyama M, Rougvie AE, Rothman JH. *C. elegans* DAF-18/PTEN mediates nutrient-dependent arrest of cell cycle and growth in the germline. *Curr Biol*. 2006; 16(8):773–9. Epub 2006/04/25. <https://doi.org/10.1016/j.cub.2006.02.073> PMID: 16631584.
 61. Hong Y, Roy R, Ambros V. Developmental regulation of a cyclin-dependent kinase inhibitor controls postembryonic cell cycle progression in *Caenorhabditis elegans*. *Development*. 1998; 125(18):3585–97. Epub 1998/08/26. <https://doi.org/10.1242/dev.125.18.3585> PMID: 9716524
 62. Lu Y, Roy R. Centrosome/Cell Cycle Uncoupling and Elimination in the Endoreduplicating Intestinal Cells of *C. elegans*. *PLoS One*. 2014; 9(10):e110958. <https://doi.org/10.1371/journal.pone.0110958> PMID: 25360893
 63. Mathies LD, Ray S, Lopez-Alvillar K, Arbeitman MN, Davies AG, Bettinger JC. mRNA profiling reveals significant transcriptional differences between a multipotent progenitor and its differentiated sister. *BMC genomics*. 2019; 20(1):427. Epub 2019/05/30. <https://doi.org/10.1186/s12864-019-5821-z> PMID: 31138122; PubMed Central PMCID: PMC6540470.
 64. Lee CS, Lu T, Seydoux G. Nanos promotes epigenetic reprogramming of the germline by down-regulation of the THAP transcription factor LIN-15B. *eLife*. 2017; 6. Epub 2017/11/08. <https://doi.org/10.7554/eLife.30201> PMID: 29111977; PubMed Central PMCID: PMC5734877.

65. Dobbelaere J, Josue F, Suijkerbuijk S, Baum B, Tapon N, Raff J. A genome-wide RNAi screen to dissect centriole duplication and centrosome maturation in *Drosophila*. *PLoS biology*. 2008; 6(9):e224. <https://doi.org/10.1371/journal.pbio.0060224> PMID: 18798690.
66. Dobbelaere J, Schmidt Cernohorska M, Huranova M, Slade D, Dammermann A. Cep97 Is Required for Centriole Structural Integrity and Cilia Formation in *Drosophila*. *Curr Biol*. 2020. Epub 2020/06/27. <https://doi.org/10.1016/j.cub.2020.05.078> PMID: 32589908
67. Matsuura K, Lefebvre PA, Kamiya R, Hirono M. Bld10p, a novel protein essential for basal body assembly in *Chlamydomonas*: localization to the cartwheel, the first ninefold symmetrical structure appearing during assembly. *J Cell Biol*. 2004; 165(5):663–71. <https://doi.org/10.1083/jcb.200402022> PMID: 15173189.
68. Carvalho-Santos Z, Machado P, Alvarez-Martins I, Gouveia SM, Jana SC, Duarte P, et al. BLD10/CEP135 is a microtubule-associated protein that controls the formation of the flagellum central microtubule pair. *Dev Cell*. 2012; 23(2):412–24. Epub 2012/08/18. <https://doi.org/10.1016/j.devcel.2012.06.001> PMID: 22898782.
69. Fu J, Lipinski Z, Rangone H, Min M, Mykura C, Chao-Chu J, et al. Conserved molecular interactions in centriole-to-centrosome conversion. *Nat Cell Biol*. 2016; 18(1):87–99. Epub 2015/11/26. <https://doi.org/10.1038/ncb3274> PMID: 26595382; PubMed Central PMCID: PMC4719191.
70. Carvalho-Santos Z, Machado P, Branco P, Tavares-Cadete F, Rodrigues-Martins A, Pereira-Leal JB, et al. Stepwise evolution of the centriole-assembly pathway. *J Cell Sci*. 2010; 123(Pt 9):1414–26. <https://doi.org/10.1242/jcs.064931> PMID: 20392737.
71. Hodges ME, Scheumann N, Wickstead B, Langdale JA, Gull K. Reconstructing the evolutionary history of the centriole from protein components. *J Cell Sci*. 2010; 123(Pt 9):1407–13. <https://doi.org/10.1242/jcs.064873> PMID: 20388734.
72. O'Connell KF, Caron C, Kopish KR, Hurd DD, Kempfues KJ, Li Y, et al. The *C. elegans* zyg-1 gene encodes a regulator of centrosome duplication with distinct maternal and paternal roles in the embryo. *Cell*. 2001; 105(4):547–58. [https://doi.org/10.1016/s0092-8674\(01\)00338-5](https://doi.org/10.1016/s0092-8674(01)00338-5) PMID: 11371350.
73. Jumper J, Evans R, Pritzel A, Green T, Figurnov M, Ronneberger O, et al. Highly accurate protein structure prediction with AlphaFold. *Nature*. 2021; 596(7873):583–9. <https://doi.org/10.1038/s41586-021-03819-2> PMID: 34265844
74. Aydogan MG, Hankins LE, Steinacker TL, Mofatteh M, Saurya S, Wainman A, et al. Centriole distal-end proteins CP110 and Cep97 influence cartwheel growth at the proximal-end of centrioles. *bioRxiv*. 2021:2021.07.08.451650. <https://doi.org/10.1101/2021.07.08.451650>
75. Li S, Armstrong CM, Bertin N, Ge H, Milstein S, Boxem M, et al. A map of the interactome network of the metazoan *C. elegans*. *Science*. 2004; 303(5657):540–3. <https://doi.org/10.1126/science.1091403> PMID: 14704431.
76. Simonis N, Rual JF, Carvunis AR, Tasan M, Lemmens I, Hirozane-Kishikawa T, et al. Empirically controlled mapping of the *Caenorhabditis elegans* protein-protein interactome network. *Nat Methods*. 2009; 6(1):47–54. Epub 2009/01/06. <https://doi.org/10.1038/nmeth.1279> PMID: 19123269; PubMed Central PMCID: PMC3057923.
77. Kraatz S, Guichard P, Obbineni JM, Olieric N, Hatzopoulos GN, Hilbert M, et al. The Human Centriolar Protein CEP135 Contains a Two-Stranded Coiled-Coil Domain Critical for Microtubule Binding. *Structure (London, England: 1993)*. 2016; 24(8):1358–71. Epub 2016/08/02. <https://doi.org/10.1016/j.str.2016.06.011> PMID: 27477386.
78. Bayless BA, Giddings TH Jr., Winey M, Pearson CG. Bld10/Cep135 stabilizes basal bodies to resist cilia-generated forces. *Mol Biol Cell*. 2012; 23(24):4820–32. Epub 2012/11/02. <https://doi.org/10.1091/mbc.E12-08-0577> PMID: 23115304; PubMed Central PMCID: PMC3521689.
79. Stenzel L, Schreiner A, Zuccoli E, Üstüner S, Mehler J, Zanin E, et al. PCMD-1 bridges the centrioles and the pericentriolar material scaffold in *C. elegans*. *Development*. 2021; 148(20). Epub 2021/09/22. <https://doi.org/10.1242/dev.198416> PMID: 34545391.
80. Nechipurenko IV, Berciu C, Sengupta P, Nicastro D. Centriolar remodeling underlies basal body maturation during ciliogenesis in *Caenorhabditis elegans*. *eLife*. 2017; 6. Epub 2017/04/16. <https://doi.org/10.7554/eLife.25686> PMID: 28411364; PubMed Central PMCID: PMC5392363.
81. Martino L, Morchoisne-Bolhy S, Cheerambathur DK, Van Hove L, Dumont J, Joly N, et al. Channel Nucleoporins Recruit PLK-1 to Nuclear Pore Complexes to Direct Nuclear Envelope Breakdown in *C. elegans*. *Dev Cell*. 2017; 43(2):157–71.e7. Epub 2017/10/25. <https://doi.org/10.1016/j.devcel.2017.09.019> PMID: 29065307.
82. McNally K, Audhya A, Oegema K, McNally FJ. Katanin controls mitotic and meiotic spindle length. *J Cell Biol*. 2006; 175(6):881–91. <https://doi.org/10.1083/jcb.200608117> PMID: 17178907.

83. Cabral G, Sanegre Sans S, Cowan CR, Dammermann A. Multiple Mechanisms Contribute to Centriole Separation in *C. elegans*. *Curr Biol*. 2013; 23(14):1380–7. Epub 2013/07/28. <https://doi.org/10.1016/j.cub.2013.06.043> PMID: 23885867.
84. Charest J, Daniele T, Wang J, Bykov A, Mandlbauer A, Asparuhova M, et al. Combinatorial Action of Temporally Segregated Transcription Factors. *Dev Cell*. 2020; 55(4):483–99.e7. Epub 2020/10/02. <https://doi.org/10.1016/j.devcel.2020.09.002> PMID: 33002421; PubMed Central PMCID: PMC7704111.
85. Gibson DG, Young L, Chuang RY, Venter JC, Hutchison CA 3rd, Smith HO. Enzymatic assembly of DNA molecules up to several hundred kilobases. *Nat Methods*. 2009; 6(5):343–5. Epub 2009/04/14. <https://doi.org/10.1038/nmeth.1318> PMID: 19363495.
86. Evans R, O'Neill M, Pritzel A, Antropova N, Senior A, Green T, et al. Protein complex prediction with AlphaFold-Multimer. *bioRxiv*. 2021:2021.10.04.463034. <https://doi.org/10.1101/2021.10.04.463034>
87. Goddard TD, Huang CC, Meng EC, Pettersen EF, Couch GS, Morris JH, et al. UCSF ChimeraX: Meeting modern challenges in visualization and analysis. *Protein science: a publication of the Protein Society*. 2018; 27(1):14–25. Epub 2017/07/16. <https://doi.org/10.1002/pro.3235> PMID: 28710774; PubMed Central PMCID: PMC5734306.
88. Oegema K, Desai A, Rybina S, Kirkham M, Hyman AA. Functional analysis of kinetochore assembly in *Caenorhabditis elegans*. *J Cell Biol*. 2001; 153(6):1209–26. <https://doi.org/10.1083/jcb.153.6.1209> PMID: 11402065.
89. Monen J, Maddox PS, Hyndman F, Oegema K, Desai A. Differential role of CENP-A in the segregation of holocentric *C. elegans* chromosomes during meiosis and mitosis. *Nat Cell Biol*. 2005; 7(12):1248–55. <https://doi.org/10.1038/ncb1331> PMID: 16273096.
90. Zanin E, Dumont J, Gassmann R, Cheeseman I, Maddox P, Bahmanyar S, et al. Affinity purification of protein complexes in *C. elegans*. *Methods Cell Biol*. 2011; 106:289–322. Epub 2011/11/29. <https://doi.org/10.1016/B978-0-12-544172-8.00011-6> PMID: 22118282; PubMed Central PMCID: PMC3319706.
91. Rappsilber J, Mann M, Ishihama Y. Protocol for micro-purification, enrichment, pre-fractionation and storage of peptides for proteomics using StageTips. *Nature protocols*. 2007; 2(8):1896–906. Epub 2007/08/19. <https://doi.org/10.1038/nprot.2007.261> PMID: 17703201.
92. Tyanova S, Temu T, Cox J. The MaxQuant computational platform for mass spectrometry-based shotgun proteomics. *Nature protocols*. 2016; 11(12):2301–19. Epub 2016/11/04. <https://doi.org/10.1038/nprot.2016.136> PMID: 27809316.
93. Webb-Robertson BJ, Wiberg HK, Matzke MM, Brown JN, Wang J, McDermott JE, et al. Review, evaluation, and discussion of the challenges of missing value imputation for mass spectrometry-based label-free global proteomics. *Journal of proteome research*. 2015; 14(5):1993–2001. Epub 2015/04/10. <https://doi.org/10.1021/pr501138h> PMID: 25855118; PubMed Central PMCID: PMC4776766.
94. Gardner ML, Freitas MA. Multiple Imputation Approaches Applied to the Missing Value Problem in Bottom-Up Proteomics. *International journal of molecular sciences*. 2021;22(17). Epub 2021/09/11. <https://doi.org/10.3390/ijms23010022> PMID: 35008458; PubMed Central PMCID: PMC8431783.
95. Frokjaer-Jensen C, Davis MW, Sarov M, Taylor J, Flibotte S, LaBella M, et al. Random and targeted transgene insertion in *Caenorhabditis elegans* using a modified Mos1 transposon. *Nat Methods*. 2014; 11(5):529–34. Epub 2014/05/14. <https://doi.org/10.1038/nmeth.2889> PMID: 24820376; PubMed Central PMCID: PMC4126194.
96. Frokjaer-Jensen C, Davis MW, Ailion M, Jorgensen EM. Improved Mos1-mediated transgenesis in *C. elegans*. *Nat Methods*. 2012; 9(2):117–8. Epub 2012/02/01. <https://doi.org/10.1038/nmeth.1865> PMID: 22290181.
97. Srayko M, Quintin S, Schwager A, Hyman AA. *Caenorhabditis elegans* TAC-1 and ZYG-9 form a complex that is essential for long astral and spindle microtubules. *Curr Biol*. 2003; 13(17):1506–11. [https://doi.org/10.1016/S0960-9822\(03\)00597-9](https://doi.org/10.1016/S0960-9822(03)00597-9) PMID: 12956952.
98. Waterhouse AM, Procter JB, Martin DM, Clamp M, Barton GJ. Jalview Version 2—a multiple sequence alignment editor and analysis workbench. *Bioinformatics (Oxford, England)*. 2009; 25(9):1189–91. Epub 2009/01/20. <https://doi.org/10.1093/bioinformatics/btp033> PMID: 19151095; PubMed Central PMCID: PMC2672624.
99. Davis MW, Morton JJ, Carroll D, Jorgensen EM. Gene activation using FLP recombinase in *C. elegans*. *PLoS Genet*. 2008; 4(3):e1000028. Epub 2008/03/29. <https://doi.org/10.1371/journal.pgen.1000028> PMID: 18369447; PubMed Central PMCID: PMC2265415.
100. Perez-Riverol Y, Csordas A, Bai J, Bernal-Llinares M, Hewapathirana S, Kundu DJ, et al. The PRIDE database and related tools and resources in 2019: improving support for quantification data. *Nucleic Acids Res*. 2019; 47(D1):D442–d50. Epub 2018/11/06. <https://doi.org/10.1093/nar/gky1106> PMID: 30395289; PubMed Central PMCID: PMC6323896.